AD-A261 050

NAVAL POSTGRADUATE SCHOOL
Monterey, California

DTIC
ELECTE
MAR 0 9 1993
S
E
D

THERMOCAPILLARY FLOW NEAR A COLD WALL

by

D. Canright

93-05034

Technical Report For Period
January 1992 - December 1992

Approved for public release; distribution unlimited

Prepared for: Naval Postgraduate School
Monterey, CA 93943

93   3 8   152

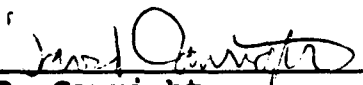NAVAL POSTGRADUATE SCHOOL
MONTEREY, CA 93943

Rear Admiral T.A. Mercer
Superintendent

Harrison Shull
Provost

This report was prepared in conjunction with research conducted for the Office of Naval Research and funded by the Office of Naval Research.
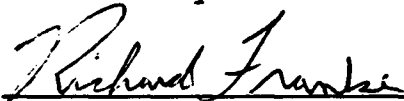
Reproduction of all or part of this report is authorized.

This report was prepared by:

D. Canright
Assistant Professor
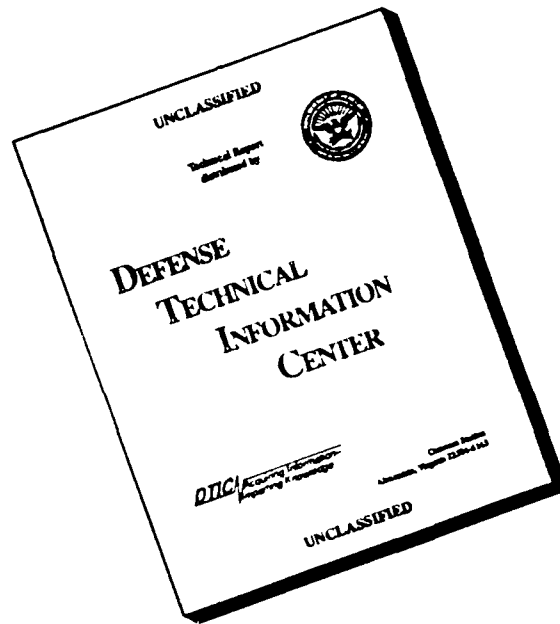
Reviewed by:

RICHARD FRANKE
Chairman

Released by:

PAUL J. MARTO
Dean of Research

DISCLAIMER NOTICE

THIS DOCUMENT IS BEST QUALITY AVAILABLE. THE COPY FURNISHED TO DTIC CONTAINED A SIGNIFICANT NUMBER OF PAGES WHICH DO NOT REPRODUCE LEGIBLY.

REPORT DOCUMENTATION PAGE		Form Approved OMB No 0704-0188

1a REPORT SECURITY CLASSIFICATION Unclassified		1b RESTRICTIVE MARKINGS .
2a SECURITY CLASSIFICATION AUTHORITY		3 DISTRIBUTION/AVAILABILITY OF REPORT Approved for public release: distribution unlimited
2b DECLASSIFICATION/DOWNGRADING SCHEDULE		
4 PERFORMING ORGANIZATION REPORT NUMBER(S) NPS-MA-93-011		5 MONITORING ORGANIZATION REPORT NUMBER(S) NPS-MA-93-011
6a NAME OF PERFORMING ORGANIZATION Naval Postgraduate School	6b OFFICE SYMBOL (If applicable) MA	7a. NAME OF MONITORING ORGANIZATION Office of Naval Research
6c. ADDRESS (City, State, and ZIP Code) Monterey, CA 93943		7b ADDRESS (City, State, and ZIP Code) 800 North Quincy St Arlington, VA 22217-5660
8a NAME OF FUNDING/SPONSORING ORGANIZATION Naval Postgraduate School	8b OFFICE SYMBOL (If applicable) MA	9 PROCUREMENT INSTRUMENT IDENTIFICATION NUMBER 622713RALDC:RA2DC
8c. ADDRESS (City, State, and ZIP Code) Monterey, CA 93943		10 SOURCE OF FUNDING NUMBERS

		PROGRAM ELEMENT NO	PROJECT NO	TASK NO	WORK UNIT ACCESSION NO

11 TITLE (Include Security Classification)
Thermocapillary Flow Near a Cold Wall

12 PERSONAL AUTHOR(S)
David Canright

13a TYPE OF REPORT Technical Report	13b TIME COVERED FROM 1-92 TO 12-92	14 DATE OF REPORT (Year, Month, Day) 1-20-93	15 PAGE COUNT 38

16 SUPPLEMENTARY NOTATION

17 COSATI CODES			18 SUBJECT TERMS (Continue on reverse if necessary and identify by block number)
FIELD	GROUP	SUB-GROUP	Thermocapillary flow

19 ABSTRACT (Continue on reverse if necessary and identify by block number)

The following model problem examines the thermocapillary feedback mechanism important at the edge of weld pools and other materials processes. A pool of liquid with a flat horizontal free surface is bounded on one side by a vertical solid wall, which is maintained at a cold temperature to unit depth, and at a warmer temperature below; far away the fluid is at the warmer temperature. Surface tension is a decreasing function of temperature, so that the surface thermal gradient drives flow toward the corner. When convection is vigorous, the flow compresses the thermal gradient which is driving the flow; this positive feedback results in small local length scales and high velocities near the corner. This problem is examined through a detailed scaling analysis and through numerical simulation for a range of parameters.

20 DISTRIBUTION/AVAILABILITY OF ABSTRACT ☒ UNCLASSIFIED/UNLIMITED ☐ SAME AS RPT ☐ DTIC USERS	21 ABSTRACT SECURITY CLASSIFICATION Unclassified	
22a NAME OF RESPONSIBLE INDIVIDUAL David Canright	22b TELEPHONE (Include Area Code) 408-656-2782	22c OFFICE SYMBOL MA/Ca

DD Form 1473, JUN 86   *Previous editions are obsolete*   SECURITY CLASSIFICATION OF THIS PAGE

THERMOCAPILLARY FLOW NEAR A COLD WALL

D. Canright
Mathematics Dept.. Code MA/Ca
Naval Postgraduate School
Monterey. CA 93943

ABSTRACT

The following model problem examines the thermocapillary feedback mechanism important at the edge of weld pools and other materi· ls processes. A pool of liquid with a flat horizontal free surface is bounded on one side by a vertical solid wall. which is maintained at a cold temperature to unit depth. and at a warmer temperature below; far away the fluid is at the warmer temperature. Surface tension is a decreasing function of temperature, so that the surface thermal gradient drives flow toward the corner. When convection is vigorous. the flow compresses the thermal gradient which is driving the flow; this positive feedback results in small local length scales and high velocities near the corner. This problem is examined through a detailed scaling analysis and through numerical simulation for a range of parameters.

_____CTED 1

THERMOCAPILLARY FLOW NEAR A COLD WALL

1. INTRODUCTION

In the processing of materials, often material is melted and resolidified. Several practical processes, e.g., welding, float-zone purification, and Czochralski crystal growth, involve a pool of molten metal with a free surface, with strong temperature gradients along the surface. Convection in the molten metal is typically vigorous and significant to the results of the process, in that it affects the size and shape of the pool, the heat transfer, the mixing of solutes, and ultimately the microstructure of the finished product. The forces driving the convection include the variation of surface tension with temperature along the surface (thermocapillary forces), buoyancy forces due to thermal (and/or solutal) expansion, and electromagnetic forces in the case of arc welding or electron beam welding. However, in many cases (e.g. laser welding) thermocapillary forces predominate, and even in cases where other forces are stronger overall, there are still important regions where the thermocapillary forces are dominant (i.e., cold corner regions: see Chen, 1987).

Consequently, there have been many theoretical studies of thermocapillary flows, primarily numerical, and a few analytical (reviews are given by Ostrach, 1982, and Davis, 1987). Cowley and Davis (1983) analyzed the (two-dimensional) thermocapillary flow near a hot wall for vigorous flow (large Marangoni number): here the fluid flows up the wall then turns and flows away along the free surface, so this would be called the hot corner problem. The numerical studies of Zebib et. al. (1985) of flow in a rectangular pool (2-D) with one hot and one cold wall, however, show that for moderate to small Prandtl numbers (e.g., metals) the cold corner region has by far the strongest effect on both the flow and the heat transfer. This result gives a different overall scaling than that of Cowley and Davis, although their local hot-corner scaling was validated. Other numerical studies (e.g., Zehr et. al., 1987), when a sufficiently fine mesh is used, show similar strong flow at the cold corner, where the flow along the free surface toward the cold wall compresses the thermal gradient, thereby enhancing the flow and the heat transfer. Great care is necessary to insure that the small length scales of this corner region are resolved numerically; this is not always the case (as noted by Chen, 1987).

Therefore, it is imperative to develop a theoretical understanding of the dynamics of the cold corner region. Being a region of intense heat transfer, the details of the flow can affect the shape of the melt pool and the cooling rate, thus the microstructure, of the material. At the least, the dependence of the length, velocity and thermal scales on the parameters (Marangoni number, Prandtl number, Capillary number) needs to be understood in order for realistic numerical models to be designed in a way to resolve the details in this important region. But as yet, such understanding is lacking. In fact, in a recent review, M. M. Chen (1987, p.552) states, "It would seem then that the structure of the cold corner flow is one of the most critical issues to be studied in the future."

To analyze the behavior of the cold corner region without all the complications of the complex geometry, phase change, and time dependence inherent in real materials processing applications, a simplified model problem will be considered, much like that of Cowley and Davis (1983), as follows. A pool of liquid has a horizontal free surface ending at a vertical wall, and the upper section of the wall is cooled; the resulting thermal gradient drives thermocapillary flow towards the cold corner. The depth and width of the pool are

assumed large compared to all local length scales (which is reasonable for practical situations with high Marangoni numbers), so the pool appears semi-infinite both horizontally and vertically.

This simplified problem is still complicated, and contains most of the features of the cold corner regions in practical processes, e.g., welds. The missing features are phase change and surface deflection, both of which could modify the geometry locally (curved wall and surface), but are unlikely to change the basic structure and scaling.

The structure of the thermal and flow fields will be examined both through a detailed scaling analysis to determine the dependence on the parameters, and through numerical simulation using two different methods.

2. PROBLEM STATMENT

A pool of incompressible Newtonian fluid is bounded on the left by a vertical solid wall, with the upper portion of the wall (to depth d) maintained at a cold temperature T_c, while the rest of the wall is at the hot ambient temperature T_h of undisturbed fluid far from the corner. (See figure 1.) Above the horizontal free surface of the liquid is an inviscid, nonconducting gas. Surface tension is assumed strong enough to keep the free surface flat (small Capillary number), but with surface tension variations due to a linear dependence on temperature. The resulting flow is assumed to be two-dimensional and steady.

Then the equations governing the thermocapillary convection in the cold corner are conservation of mass, momentum, and energy:

$$\nabla \cdot \mathbf{u} = 0 \tag{2.1}$$

$$\rho\, \mathbf{u} \cdot \nabla \mathbf{u} = -\nabla p + \mu\, \nabla^2 \mathbf{u} \tag{2.2}$$

$$\rho c_p\, \mathbf{u} \cdot \nabla T = k\, \nabla^2 T \tag{2.3}$$

with the boundary conditions:

$$\text{at} \quad y = 0: \quad T_y = 0, \quad v = 0, \quad \mu u_y = \gamma T_x \tag{2.4a,b,c}$$

$$\text{at} \quad x = 0: \quad T = \begin{cases} T_c, & y < d \\ T_h, & y > d \end{cases}, \quad u = v = 0 \tag{2.5a,b,c}$$

$$\text{as} \quad x, y \to \infty: \quad T \to T_h, \quad u, v \to 0 \tag{2.6a,b,c}$$

Here $\mathbf{u}$ is the velocity vector with components u and v in the x (horizontally rightward) and y (vertically downward) directions, p is pressure, T is temperature, ρ is density, μ is viscosity, c_p is specific heat, k is thermal conductivity, and γ (assumed constant and negative) is the derivative of the surface tension with respect to temperature. The boundary conditions specify that the wall is piecewise isothermal with no fluid slip, and the flat free surface is thermally insulated, with thermocapillary forcing.

The equations can be nondimensionalized by scaling lengths by d, temperature differences by $\Delta T \equiv T_h - T_c$, and velocities by $u_s \equiv \gamma\, \Delta T / \mu$. The resulting dimensionless equations are:

$$\nabla \cdot \mathbf{u} = 0 \tag{2.7}$$

$$R\, \mathbf{u} \cdot \nabla \mathbf{u} = -\nabla p + \nabla^2 \mathbf{u} \tag{2.8}$$

$$M\, \mathbf{u} \cdot \nabla T = \nabla^2 T \tag{2.9}$$

2

with the boundary conditions:

$$\text{at} \quad y = 0: \quad T_y = 0, \quad v = 0, \quad u_y = T_x \qquad (2.10\text{a,b,c})$$

$$\text{at} \quad x = 0: \quad T = \begin{cases} -1, & y < 1 \\ 0, & y > 1 \end{cases}, \quad u = v = 0 \qquad (2.11\text{a,b,c})$$

$$\text{as} \quad x, y \to \infty: \quad T \to 0, \quad u, v \to 0 \qquad (2.12\text{a,b,c})$$

where $\mathbf{u}$, etc. from here on denote the dimensionless quantities. The two dimensionless parameters are the Marangoni number $M \equiv u_s d / \kappa$ and the Reynolds number $R \equiv u_s d / \nu$, where $\kappa = k / \rho c_p$ is the thermal diffusivity and $\nu = \mu / \rho$ is the kinematic viscosity. Their ratio gives the Prandtl number: $P \equiv \nu / \kappa = M/R$.

For the numerical solutions below, it is convenient to eliminate the pressure by adopting a stream-function/vorticity formulation for the flow:

$$R \, \mathbf{u} \cdot \nabla \omega = \nabla^2 \omega \qquad (2.13)$$

$$\omega = -\nabla^2 \Psi \qquad (2.14)$$

$$u = \Psi_y, \quad v = -\Psi_x \qquad (2.15\text{a,b})$$

where Ψ is the stream function and ω is the vorticity, with the flow boundary conditions

$$\text{at} \quad y = 0: \quad \Psi = \Psi_x = 0, \quad \omega = -T_x \qquad (2.16\text{a,b,c})$$

$$\text{at} \quad x = 0: \quad \Psi = \Psi_x = \Psi_y = 0 \qquad (2.17\text{a,b,c})$$

$$\text{as} \quad x, y \to \infty: \quad \Psi, \omega \to 0 \qquad (2.18\text{a,b})$$

3. SCALING ANALYSIS AND REGIMES OF BEHAVIOR

The structure of the thermal and flow fields can take on different forms, depending on the values of the two governing parameters, the Marangoni number M, which measures the importance of thermal convection relative to thermal diffusion, and the Prandtl number P, which is the ratio of viscous to thermal diffusion, a material property. (Equivalently, one could use Reynolds number $R = M/P$ as the second parameter, the ratio of inertial to viscous forces.) Here we derive the appropriate dimensionless scales for the four different asymptotic regimes of behavior.

To examine the dominant balances in the cold corner, three scales suffice: the horizontal length scale l for the thermal gradient along the surface, the vertical viscous length scale δ for the velocity shear at the surface (which turns out to be the same scale as for the velocity shear on the wall), and the velocity scale U for flow along the surface. The vertical thermal length scale is determined by the boundary condition on the wall, and so is $O(1)$. The thermocapillary stress condition (2.10c) scales as:

$$\frac{U}{\delta} \sim \frac{1}{l} \qquad (3.1)$$

so that $U \sim \delta / l$. In the energy and vorticity equations (2.9 and 2.13), the terms for convection in each direction scale the same, but not so for diffusion, and by (2.16), the

3

surface vorticity scale is $1/l$. so (2.9) and (2.13) scale as:

$$M \frac{U}{l} \sim \frac{1}{l^2} + 1 \tag{3.2}$$

$$R \frac{U}{l^2} \sim \frac{1}{l^3} + \frac{1}{l\delta^2} \tag{3.3}$$

For small enough M, thermal convection is negligible. implying $l \sim 1$. and the thermal field is essentially conductive. decoupled from the flow. But for large enough M convection becomes important. and the strong surface flow toward the wall compresses the thermal gradient along the surface, which in turn strengthens the local driving force for the flow. This reduces the horizontal thermal length scale l to the point that thermal diffusion away from the wall balances convection toward the wall. so the local *effective* Marangoni number is order unity: $M_{eff} \equiv MUl \sim 1$. Then the externally imposed length scale (dimensional d above) is no longer directly relevant to the compressed cold corner region. (In this case, the local importance of inertia is better indicated by whether viscous or thermal diffusion is more efficient, i.e., by P rather than R.)

Similarly, for small enough R, inertia is negligible everywhere, implying $\delta \sim l$. and the flow is dominated by viscous forces. For large enough R inertial forces become dominant and viscous effects are confined to boundary layers of thickness $\delta \ll l$ along the surface and the wall, where the local effective Reynolds number $R_{eff} \equiv RU\delta^2/l \sim 1$. (Both layers are of comparable thickness because the pressure field outside the layers has the same length scale in both directions.) The above gives the scaling for each regime.

When the thermal field is conductive and the flow field dominated by viscous forces ($M \ll 1$ and $R \ll 1$. or $P \gg M$). all three scales are of order unity: $l \sim 1$. $\delta \sim 1$. $U \sim 1$. Thus in this case (only). the scaling used in the nondimensionalization is appropriate everywhere. Within this regime. the solution is fully two-dimensional with no fine structure and is nearly independent of the parameters.

For the conductive case with inertial flow, the additional resistance of inertia reduces both the velocity scale and the viscous length scale: $U \sim \delta \sim R^{-\frac{1}{3}}$ (while $l \sim 1$ still). This reduced velocity also reduces the effective Marangoni number. such that this regime applies when $M \ll R^{\frac{1}{3}}$, or $M \ll P^{-\frac{1}{2}}$, with $R \gg 1$. or $P \ll M$. (Note that this gives the same boundary layer scaling as Zebib et al., 1985, except they made an error on the passive wall layers. as pointed out by Chen, 1987.) Here the vorticity generated by the shear stresses on the surface and the wall are confined to the thin boundary layers.

When thermal convection is important but inertia is not ($M \gg 1$ and $P \gg 1$). surface thermal varitions are compressed to a narrow region. beyond which the thermocapillary forcing is small, so $\delta \sim l \sim M^{-1}$ and $U \sim 1$. However, the strong inward flow along the surface turns downward and *away* from the no-slip wall (and weakens rapidly with distance). such that *no* thermal boundary layer is formed on the wall: rather, vertical and horizontal variations are comparable.

The most important regime for materials processing is where thermal convection is important and $P \ll 1$. the latter being generally true for metals. In this case. within the compressed thermal region there are thin viscous boundary layers along the surface and wall. Then $l \sim M^{-1}P^{-\frac{1}{2}}$, $\delta \sim M^{-1}$. and $U \sim P^{\frac{1}{2}}$. i.e., the additional resistance of inertia

4

decreases the velocity scale and thus increases the thermal scale by a factor of $\sqrt{P}$ relative to the purely viscous case. Again the reduced velocity changes the thermal convection scaling, and large Marangoni number here means $M \gg P^{-\frac{1}{2}}$.

The approximate divisions between the four asymptotic regimes are shown in figure 2. For a material of small P, as M is increased from zero, at first the temperature field is conductive and the flow dominated by viscous forces, then the flow becomes primarily inertial and viscous boundary layers form, and finally thermal convection becomes dominant, shrinking all local length scales in the corner.

4. VISCOUS CORNER REGION

There is a region in the corner, for any M and P, where viscous stresses from the wall limit the flow and both inertia and thermal convection are negligible, so the temperature is a linear function along the surface. Locally the thermocapillary stress is constant, and the flow is given by a similarity solution (Moffatt, 1964, although the published version is incorrect).

If the flat free surface makes an angle α with the solid wall, then a constant unit surface shear stress toward the corner gives

$$\Psi(r,\theta) = \frac{r^2}{4} \frac{[(\sin 2\alpha - 2\alpha)(\cos 2\theta - 1) - (\cos 2\alpha - 1)(\sin 2\theta - 2\theta)]}{\sin 2\alpha - 2\alpha \cos 2\alpha} \tag{4.1}$$

where r and θ are polar coordinates, with θ increasing from the wall to the free surface (see figure 1). In the special case here, $\alpha = \frac{\pi}{2}$, and

$$\Psi(r,\theta) = r^2 \left[\frac{1}{4}(1 - \cos 2\theta) + \frac{1}{2\pi}(\sin 2\theta - 2\theta) \right] \tag{4.2a}$$

$$\mathbf{u} = r \left\{ \left[\frac{1}{2}\sin 2\theta + \frac{1}{\pi}(\cos 2\theta - 1) \right] \hat{r} \right.$$
$$\left. - \left[\frac{1}{2}(1 - \cos 2\theta) + \frac{1}{\pi}(\sin 2\theta - 2\theta) \right] \hat{\theta} \right\} \tag{4.2b}$$

$$\omega = 1 - \frac{4}{\pi}\theta \tag{4.2c}$$

$$p - p_0 = \frac{4}{\pi}\ln r \tag{4.2d}$$

where $\hat{r}$ and $\hat{\theta}$ are unit vectors in the coordinate directions, and p_0 is some reference pressure. Figure 3 shows the streamlines for this similarity flow. The zero-vorticity contour extends from the corner at a $45°$ angle, dividing the negative vorticity on the surface from the positive vorticity on the wall.

This is the form of the flow in the cold corner on the smallest length scale, where all the above flow quantities would be multiplied by $T_x(0,0)$ (which scales as $1/l$). The velocity grows linearly with distance r from the corner and the local length scale is r, which can be used to estimate the range over which the similarity solution is applicable. For the two viscous-flow regimes mentioned above, the linear-temperature approximation requires $r \ll l$, so for the conductive regime $r \ll 1$ while for the convective regime $r \ll M^{-1}$.

5

For the two inertial-flow regimes, the more restrictive condition is that locally inertia is negligible, and the local velocity scale is r/l, so we must have $r^2 \ll l/R$: in the conductive regime this implies $r \ll R^{-\frac{1}{2}}$, while in the convective regime the range is $r \ll P^{\frac{1}{4}}M^{-1}$, or $r/l \ll P^{\frac{3}{4}}$.

This gives an estimate of the resolution required for a numerical model to resolve all the details of the cold corner flow. Because of the corner singularity in ω and p, spectral methods would be inappropriate; instead, finite-difference or finite-element methods could be used. Then if the first grid point is in the similarity range, no details of the velocity field in the corner will be lost. In addition, the similarity form may be useful as a "matching" type boundary condition for the singularity at the origin.

5. GREEN'S FUNCTION METHOD FOR VISCOUS CASE: $R \to 0$

When the Reynolds number is sufficiently small, inertia is negligible throughout the flow field, and to lowest approximation the flow is governed by the biharmonic equation:

$$\nabla^2 \left(\nabla^2 \Psi \right) = 0 \tag{5.1}$$

Then the flow everywhere depends only on the instantaneous thermal gradient along the surface (even if the flow is unsteady). This allows the flow field to be represented using the Green's function for a point force near a rigid wall, directed toward the wall (see, e.g., Hasimoto & Sano, 1980, or Blake, 1971).

The Green's function for the stream function due to a unit (dimensionless) force in the negative x direction applied on the surface at the point $(\xi, 0)$ is:

$$G(x, y, \xi) \equiv \frac{1}{2\pi} \left[y \ln \left(\frac{r_+}{r_-} \right) - \frac{2\,xy\xi}{r_+^2} \right] \tag{5.2a}$$

where

$$r_+ \equiv \sqrt{(x+\xi)^2 + y^2}, \quad r_- \equiv \sqrt{(x-\xi)^2 + y^2} \tag{5.2b}$$

The flow field due to such a point force at $\xi = 1$ is shown in figure 4. (Note that all distances scale with ξ.) The far field ($r \gg \xi$) can be used as an approximation to the viscous thermocapillary flow at large enough distances that the distributed forcing of the thermal gradient can be replaced by a point force near the wall. It can be shown that in the far-field the zero vorticity contour approaches an angle of $\frac{\pi}{3}$ from the surface. As r increases, the velocity decays rapidly as $\mathbf{u} \sim O(r^{-2})$.

This rapid decay of velocity has the consequence that *no* thermal boundary layer forms on the wall. While this result only applies directly when inertia is negligible, one would expect that the same order of decay applies to the inertial case in the far field, by analogy with the Squire-Landau jet (Landau, 1944, and Squire, 1951) where the velocity due to an isolated point force decays like $\mathbf{u} \sim O(r^{-1})$ for all Reynolds numbers. Note also that near the wall (except near the surface), the flow is *away* from the wall. Hence, though the surface temperature gradient may be highly compressed from vigorous convection, there is no thermal boundary layer along the wall, i.e., vertical and horizontal temperature variations are expected to be of the same order. This is in marked contrast with the seemingly comparable case of a hot corner. There the flow tends to expand the surface

6

thermal gradient over long distance, so the forcing is similar to a distributed line force, and thermal boundary layers form both on the wall and the surface (Cowley and Davis, 1983). This difference between concentrated forcing and distributed forcing changes the fundamental character of the flow.

Using the Green's function, then the stream function, velocity components, and vorticity in the viscous thermocapillary flow are given by:

$$\Psi(x,y) = \frac{1}{2\pi} \int_0^\infty T'(\xi) \left[y \ln\left(\frac{r_+}{r_-}\right) - \frac{2xy\xi}{r_+^2} \right] d\xi \tag{5.3a}$$

$$u(x,y) = \frac{1}{2\pi} \int_0^\infty T'(\xi) \left[\ln\left(\frac{r_+}{r_-}\right) + y^2\left(\frac{1}{r_+^2} - \frac{1}{r_-^2}\right) - \frac{2x\xi}{r_+^2}\left(1 - \frac{2y^2}{r_+^2}\right) \right] d\xi \tag{5.3b}$$

$$v(x,y) = \frac{1}{2\pi} \int_0^\infty T'(\xi) \left[y\left(\frac{x+\xi}{r_+^2} - \frac{x-\xi}{r_-^2}\right) - \frac{2y\xi}{r_+^2}\left(1 - \frac{2x(x+\xi)}{r_+^2}\right) \right] d\xi \tag{5.3c}$$

$$\omega(x,y) = \frac{1}{2\pi} \int_0^\infty T'(\xi) \left[2y\left(\frac{1}{r_+^2} - \frac{1}{r_-^2}\right) - \frac{8\xi(x+\xi)y}{r_+^4} \right] d\xi \tag{5.3d}$$

using the shortened notation $T'(x) \equiv T_r(x,0)$.

To calculate the steady flow for various values of Marangoni number (with $R = 0$), the time-dependent equation for the temperature field was explicitly integrated in time until the steady state was reached. A finite square domain on a uniform grid was used, where on the artificial boundaries, diffusion across the boundaries is neglected and where convection is inward the fluid outside is assumed to be at zero temperature. The effects of these artificial boundaries on the cold corner are presumably small if the boundaries are several units away, since the thermal field decays quickly with distance. Central finite differences were used, with upwind differencing for the convective terms. The velocity at each point was evaluated from the above integrals (5.3b,c), using an analytic approximation around the singularity at $(x,0)$, and elsewhere using the trapezoidal rule with first-order differences for the thermal gradient, as central differences here resulted in a numerical instability.

The results for a range of M are shown in figure 5. The transition from the primarily conductive regime to the convective regime as M increases is apparent. As the surface gradient becomes more compact, the strong downward convection away from the corner extends the thermal region into a sort of broad diagonal plume; no thermal boundary layer forms even for large M. (Where the isotherms intersect the artificial boundaries, slight local distortion due to the artificial boundary conditions is apparent.) For large M, the flow outside the cold corner is qualitatively similar to the flow from a point source (see figure 4).

6. NUMERICAL SOLUTIONS FOR FULL SYSTEM

When inertia is not negligible, the full coupled nonlinear equations must be solved. Unlike the Green's function approach, this requires flow boundary conditions at the artificial boundaries of the computational domain; here these boundaries are assumed to be impermeable and shear-free, as well as isothermal. These conditions constrain both the thermal and flow fields (compared to the Green's function method), enhancing recirculation and preventing long thermal plumes. Still, with the artificial boundaries several units away, their effects on the cold corner are expected to be small.

7

Again, the numerical method involves stepping the unsteady equations forward in time until steady state is reached. At each time step, the convection-diffusion equations for temperature (2.9) and vorticity (2.13) are solved by the Alternating-Direction Implicit (ADI) scheme, where the convective terms are evaluated by the Eulerian-Lagrangian Method (ELM, see Cheng et al., 1984) using the velocity field from the old stream function and upwind bilinear interpolation. (The ADI method avoids diffusive numerical instability, so the time step is only limited by convective stability.) After several time steps, the Poisson equation for the stream function (2.14) is solved by Gauss-Seidel iteration with Successive Over-Relaxation (SOR). Steady state is assumed when the pointwise RMS change in stream function is below a certain tolerance.

A non-uniform Cartesian grid was employed. (The program allows arbitrary spacing of points in each direction.) Using a three-point difference scheme, only first-order accuracy is possible for the second derivatives; the differencing employed becomes second-order in the limit of uniform spacing. Specifically, the following one-dimensional difference formulae were used (derived from Taylor series):

$$f' = \frac{-dx_+}{dx_-(dx_+ + dx_-)} f_- + \frac{dx_+ - dx_-}{dx_+ dx_-} f + \frac{dx_-}{dx_+(dx_+ + dx_-)} f_+$$
$$+ O(f''' dx_+ dx_-) \tag{6.1a}$$

$$f'' = \frac{2}{dx_-(dx_+ + dx_-)} f_- + \frac{-2}{dx_+ dx_-} f + \frac{2}{dx_+(dx_+ + dx_-)} f_+$$
$$+ O(f'''(dx_+ - dx_-)) \tag{6.1b}$$

where dx_- and dx_+ are the distances to the grid points below and above the current point, with f_- and f_+ the corresponding values of the function.

The grid spacing in each direction was chosen to have a closely packed region of uniform spacing by the surface or wall, a widely spaced region of uniform spacing out near the artificial boundaries, and in between a region of smoothly (exponentially) changing spacing. This was generated by applying the following function to a uniform grid (in ξ, say):

$$\frac{x}{x_{max}} = f(\xi) = \begin{cases} \ln r\,\xi/D, & 0 \le \xi < \xi_1 \\ (\xi_2 - \xi_1)\,r^{(\xi-\xi_1)/(\xi_2-\xi_1)}/D\,r^{\xi_2-\xi_1-\ln r\xi_1}, & \xi_1 \le \xi < \xi_2 \\ 1 - r\ln r\,(1-\xi)/D, & \xi_2 \le \xi \le 1 \end{cases} \tag{6.2}$$

where r is a parameter giving the ratio of outer to inner spacing. ξ_1 and ξ_2 are parameters delineating the three regions. $D = (r-1)(\xi_2 - \xi_1) + \ln r(r + \xi_1 - r\xi_2)$, and x_{max} is the position of the artificial boundary.

It was found that, even when the time step easily satisfied convective stability requirements, nonetheless instabilities developed in the vorticity near the wall. Several different formulations for the wall boundary condition on vorticity were tried, to no avail. However, by under-relaxing the changes in wall vorticity only during the initial adjustment period, the instability was eliminated. The formula used to calculate the vorticity at the wall (without under-relaxation) from the stream function is

$$\omega_0 = \frac{2(\Psi_1 - \Psi_2)}{x_2^2 - x_1^2} + O(\Psi''' x_2) \tag{6.3}$$

8

where subscripts 0, 1, and 2 refer to the wall and the first two grid points. While only first-order, this formulation is independent of Ψ_0 and thus avoids re-using the boundary condition for Ψ.

Results are shown in figures 6 and 7 for $P = 1$ and $P = 0.01$, for a variety of M. The conductive, viscous regime is represented by the case $M = 0.01$, $P = 1$ (figure 6a). For $P = 1$, with increasing M, the surface thermal gradient becomes compressed (similar to the $P = \infty$ case computed by Green's functions) along with the vorticity on the surface. However, inertia is no longer negligible, and so the flow down the wall has less of an outward component. Also, the artificial boundaries modify the "plume," keeping it from the boundaries and turning it upward due to the recirculation. For $P = 0.01$ (as typical in liquid metals), with increasing M inertial effects confine the vorticity, forming clear viscous boundary layers, before thermal convection becomes strong. Also, a counter-rotating cell forms in the lower part of the domain. As thermal convection compresses the surface gradient, the surface viscous boundary layer remains limited to the cold corner. Note that for large M and small P, the thermal length scale is small compared to the overall domain, and the viscous length scale is small compared to the thermal scale, imposing severe (local) resolution requirements on any numerical model.

The numerical results for $P = 1$ and $P = 0.01$ are compared with the scaling analysis in figure 8. The thermal length scale (or rather $1/l$) is estimated from the thermal gradient T_x at the wall (based on the first grid point along the surface). The velocity scale (U) is estimated from the maximum velocity u_{max} at a grid point on the surface (though the actual maximum might be expected to fall between grid points). The viscous length scale (δ) is approximated by the position x_{max} of the grid point with the maximum velocity. For $P = 1$, the transition is apparent from the conductive viscous regime (where l, U, and δ are nearly independent of M) to the convective viscous regime (where $l \propto M^{-1}$ and $\delta \propto M^{-1}$, with U roughly constant). For $P = 0.01$, two transitions are seen, from the conductive viscous regime to the conductive inertial regime (l nearly constant, $U \propto M^{-1/3}$, and $\delta \propto M^{-1/3}$), to the convective inertial regime ($l \propto M^{-1}$, $\delta \propto M^{-1}$, U nearly constant).

7. DISCUSSION AND CONCLUSIONS

The practical importance of thermocapillary convection in materials processing, along with the complications inherent in typical processes (e.g. curved interfaces, phase change, etc.), insure that numerical simulations will remain one of the main theoretical tools for understanding such systems. This work predicts, a priori, the resolution requirements for such numerical models to accurately represent the high heat transfer and rapid velocity variations in the cold corner region.

The structure of the corner depends on two dimensionless parameters indicating the driving force for convection and relative importance of viscosity: the Marangoni number M (based on the overall temperature difference, overall thermal length scale, and material properties) and the Prandtl number P (a material property). Hence there are four asymptotic regimes (shown in figure 2) depending on whether thermal convection and inertial forces are locally important. For large-P materials (e.g., organics), the corner flow is dominated by viscous forces, and for large M the surface thermal variations are compressed, i.e., the local length scale is decreased (and heat transfer increased). For small-P materials (e.g., metallics), inertia becomes important before thermal convection with increasing

9

M, and thin viscous boundary layers form within the thermal region. When M is large (compared to $P^{-1/2}$), three levels of length scales must be resolved (overall, thermal, and viscous), a severe requirement on numerical models.

The scaling was derived from a simple problem designed to isolate the feedback mechanism of the cold corner. Numerical calculations by two methods for closely related problems (where the corner is necessarily less isolated due to the finite domain) illustrate the changing structure of the cold corner and show the details of the transitions between the asymptotic regimes. The numerical results are consistent with the scaling analysis.

One surprising result, in contrast with the hot corner problem of Cowley and Davis (1983), is that no thermal boundary layers form. This difference is due to the forcing being limited to a relatively concentrated region in the cold corner, while for the hot corner the forcing is distributed over an extended region (the horizontal thermal variations being extended by convection).

To compare with the numerical results of Zebib et al. (1985) for $P = 1$, note the different boundary conditions: their domain had a (flat) free surface, a hot and a cold no-slip wall, and an insulated no-slip bottom. Then even when the cold corner was highly compressed, there were still significant thermal variations along most of the surface due to the hot wall, so the overall scaling is similar to the conductive inertial case here. And apparently even their cold corner was modified by the external bulk flow, for their maximum vorticity scaled as $\omega \propto M^{2/3}$, whereas here $\omega \propto M$. (The resolution requirements derived here can thus be considered conservative.) Hence one important question remaining is under what conditions can the cold corner be considered locally determined (as it is here).

In real materials processes, the surface is free to deflect, and the position and shape of the solid-liquid interface depends on the thermal field. These effects greatly complicate the problem geometrically, yet the dominant dynamic balance should remain that considered here. Future work will investigate these effects in the cold corner.

8. ACKNOWLEDGMENTS

REFERENCES

J. R. Blake, "A note on the image system for a stokeslet in a no-slip boundary," *Proc. Camb. Phil. Soc.*, **70**:303-310 (1971).

C. Chan, J. Mazumder, and M. M. Chen, "Effect of surface tension gradient driven convection in a laser melt pool: Three-dimensional perturbation model," *J. Appl. Phys.*, **64**:6166-6174 (1988).

M. M. Chen, "Thermocapillary convection in materials processing," from *Interdisciplinary Issues in Materials Processing and Manufacturing* (ASME), ed.: S. K. Samanta, R. Komandiri, R. McMeeking, M. M. Chen, A. Tseng, pp.541-557 (1987).

S. J. Cowley and S. H. Davis, "Viscous thermocapillary convection at high Marangoni number," *J. Fluid Mech.*, **135**:175-188 (1983).

S. H. Davis, "Thermocapillary Instabilities," *Ann. Rev. Fluid Mech.*, **19**:403-435 (1987).

H. Hasimoto and O. Sano. "Stokeslets and eddies in creeping flow." *Ann. Rev. Fluid Mech..* **12**:335-363 (1980).

L. Landau.*Doklady Acad. Sci.. U.R.S.S..* **43**:286 (1944).

H. K. Moffatt. "Viscous and resistive eddies near a sharp corner." *J. Fluid Mech..* **16**:1 (1964).

S. Ostrach. "Low Gravity Fluid Flows." *Ann. Rev. Fluid Mech..* **14**:313-345 (1982).

A. K. Sen and S. H. Davis. "Steady thermocapillary flows in two-dimensional slots." *J. Fluid Mech..* **121**:163-186 (1982).

H. B. Squire, *Quart. J. Mech. Appl. Math..* **4**:321 (1951).

A. Zebib, G. M. Homsy. and E. Meiburg. "High Marangoni number convection in a square cavity." *Phys. Fluids.* **28**:3467-3476 (1985).

R. Zehr. M. M. Chen. and J. Mazumder. "Thermocapillary Convection of a Differentially Heated Cavity at High Marangoni Numbers." ASME Paper No. 87-HT-229. National Heat Transfer Conference. Pittsburgh. PA. Aug. 10-12. 1987.

FIGURE CAPTIONS

Figure 1. Problem Formulation: a liquid quarter-space is bounded above by a flat free surface subject to thermocapillary forcing, and is bounded on the left by a rigid vertical wall, at temperature T_c to depth d and at the warmer temperature T_h below, which is also the ambient temperature of the undisturbed fluid far away.

Figure 2. Asymptotic Regimes: the four different asymptotic behaviors correspond to whether the thermal field is controlled primarily by convection or by conduction, and whether the flow is dominated by viscous or inertial forces.

Figure 3. Viscous Corner Flow: streamlines (solid, black) and vorticity contours (dashed, light gray) for the self-similar solution valid where the surface temperature is approximately linear and inertia is negligible.

Figure 4. Green's Function: streamlines (solid, black) and vorticity contours (dashed, light gray) for the non-inertial flow due to a point force on the surface at $(1,0)$, directed toward the wall. The flow is recirculating and decays rapidly with distance.

Figure 5. Numerical Results for $R \rightarrow 0$ ($P \rightarrow \infty$): velocity vectors and isotherms (solid, dark gray) of numerical solutions using the Green's function formulation, for a range of Marangoni numbers. On the artificial boundaries (bottom and right), normal thermal diffusion is neglected and incoming fluid is assumed isothermal. (a) $M = 10$; (b) $M = 30$; (c) $M = 100$; (d) $M = 300$; (e) $M = 1000$.

Figure 6. Numerical Results for $P = 1$: isotherms (solid, dark gray), streamlines (thin, black) and vorticity contours (dashed, light gray), for the numerical solution of the full coupled system. The artificial boundaries (bottom and right) are assumed isothermal, impenetrable, and shear-free. (a) $M = 0.01$; (b) $M = 10$; (c) $M = 30$; (d) $M = 100$; (e) $M = 300$; (f) $M = 1000$; (g) detail of $M = 1000$.

Figure 7. Numerical Results for $P = 0.01$: see previous caption. (a) $M = 1$; (b) $M = 10$; (c) $M = 100$; (d) detail of $M = 100$; (e) $M = 1000$; (f) detail of $M = 1000$; (g) $M = 10,000$; (h) detail of $M = 10,000$.

Figure 8. Summary of Numerical Scales: wall temperature gradient T_x (diamonds), maximum velocity u_{max} (triangles), and position x_{max} of maximum velocity (stars), as functions of Marangoni number M, from numerical solutions of full system. Lines of slope 1, -1, and -1/3 are shown for comparison with scaling analysis. (a) $P = 1$; (b) $P = 0.01$.

Figure 1

AIR

$T_y = 0, \ v = 0, \ \mu \, u_y = \gamma \, T_x$

x

y

r θ

SOLID

LIQUID

$T = T_c$
$u = v = 0$

flow direction

$y = d$

$T \to T_h$
$u, v \to 0$

$T = T_h$
$u = v = 0$
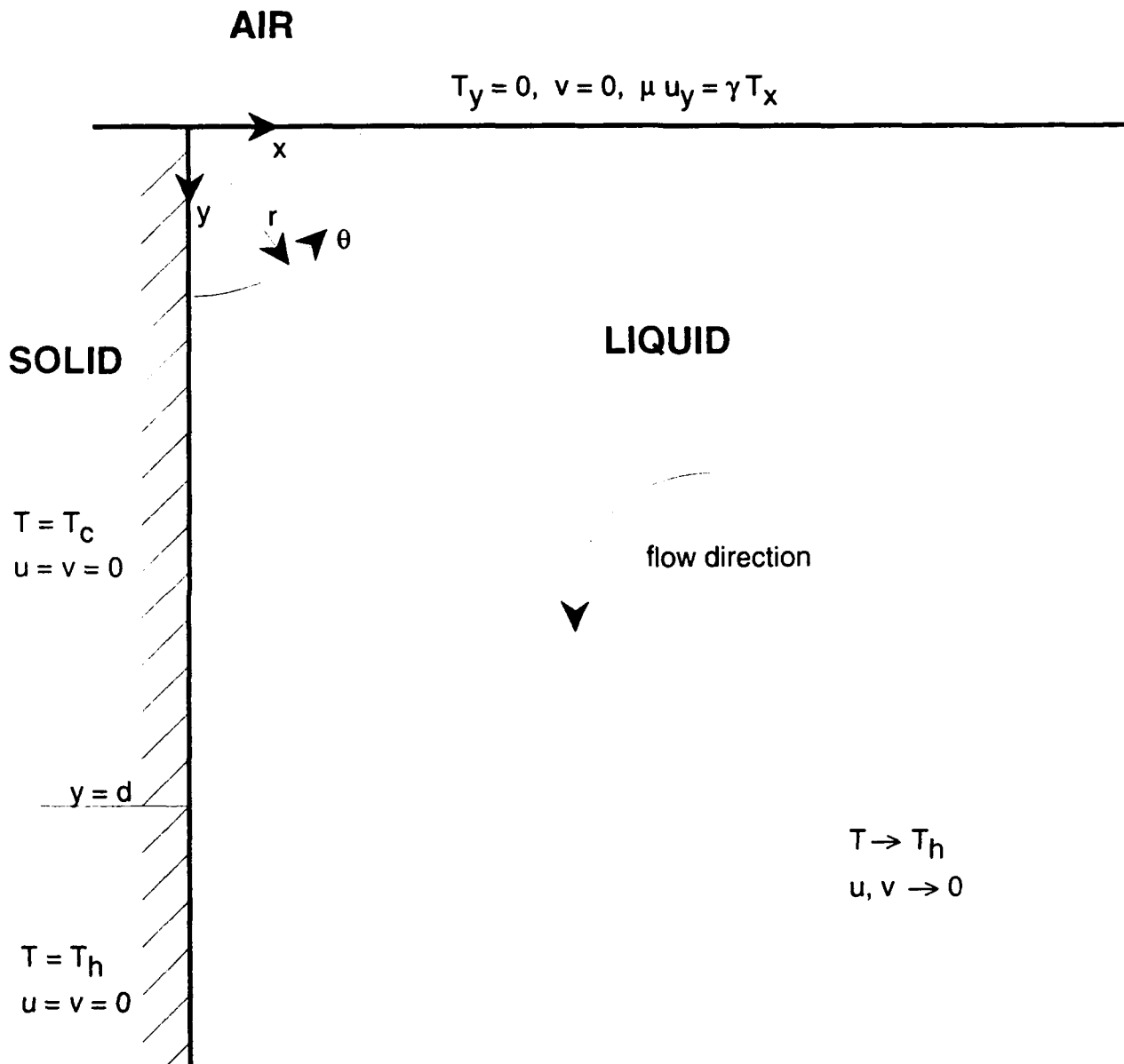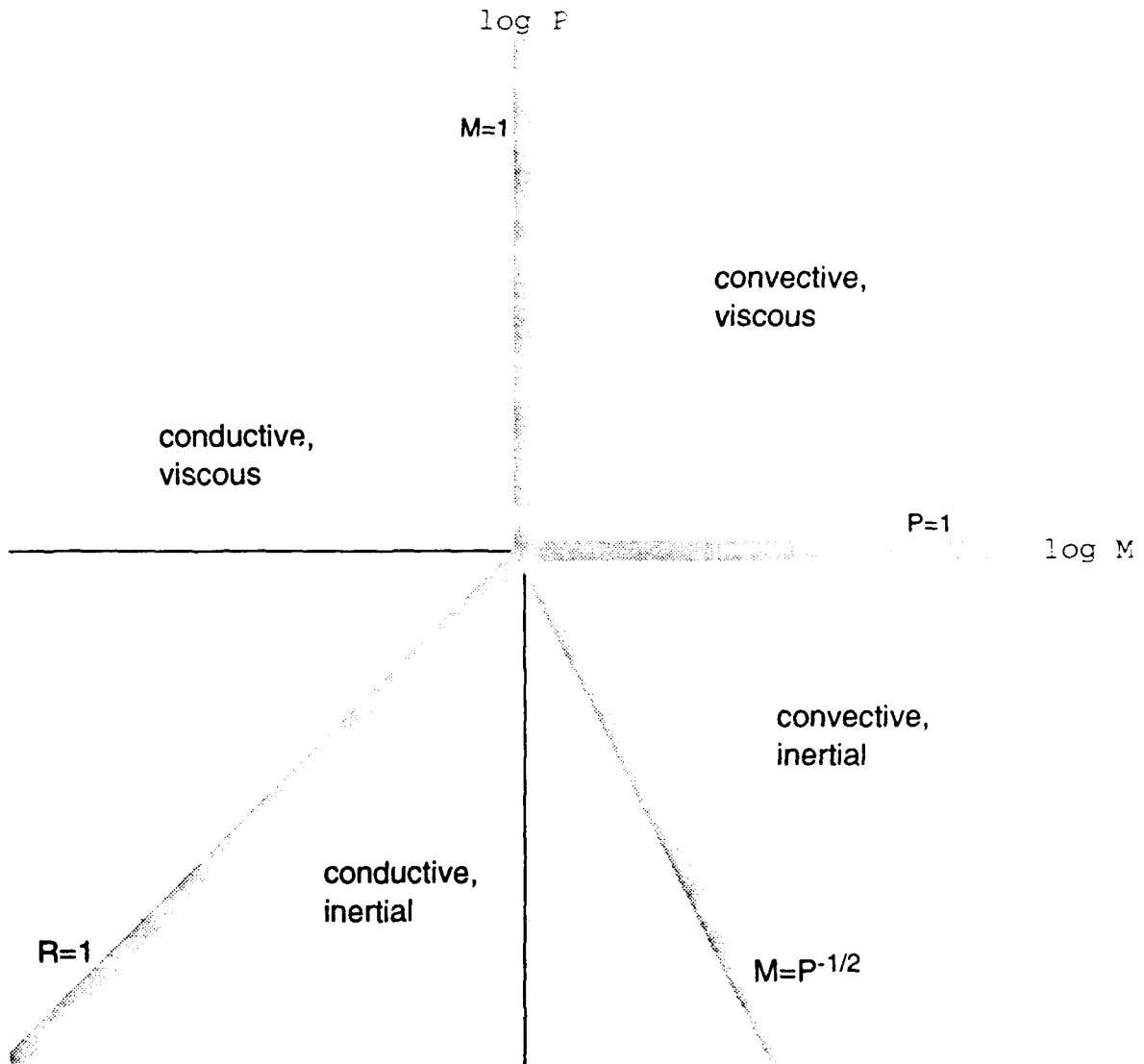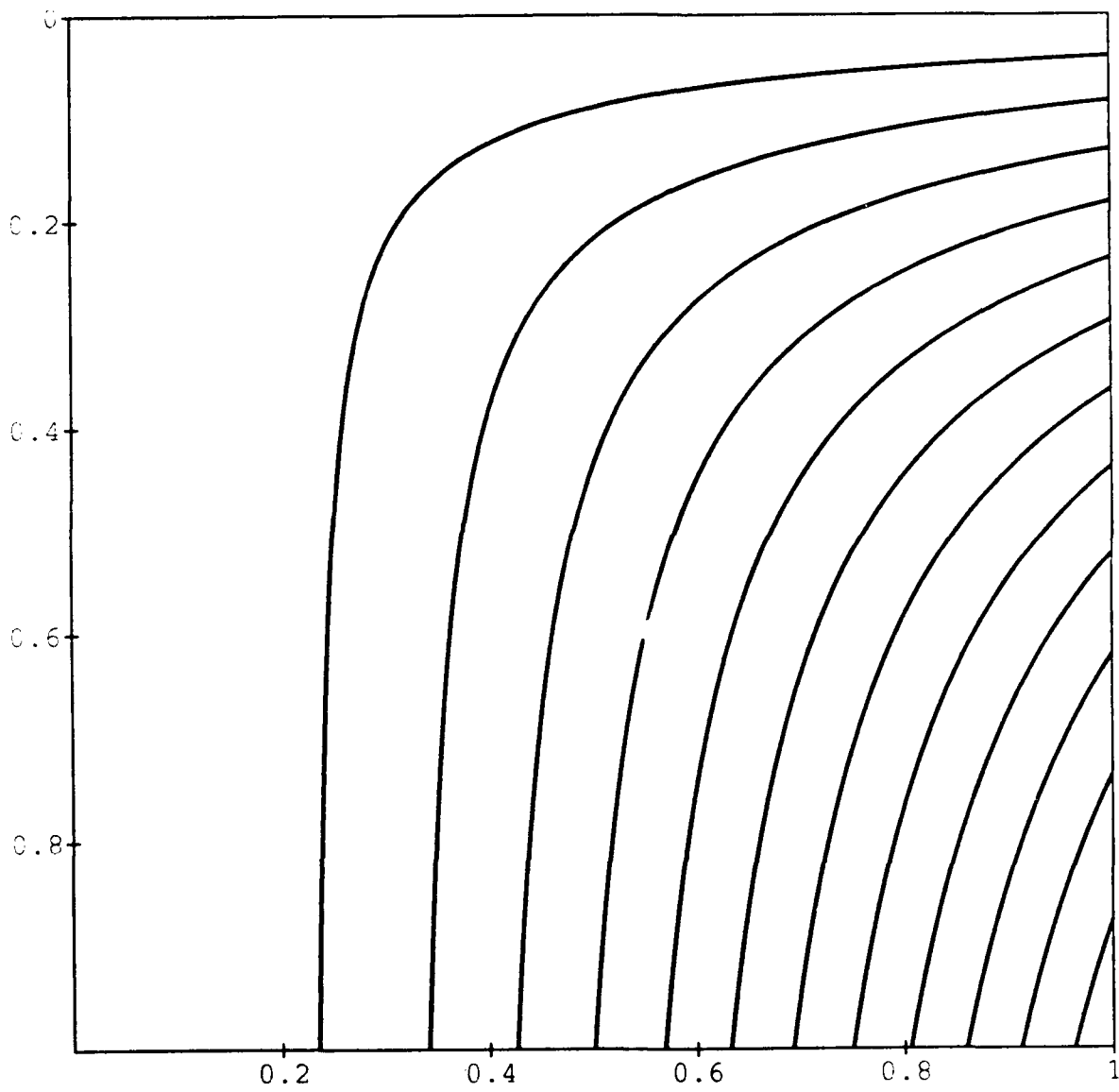
Figure 2

Figure 3

Figure 4

Figure 5a

$$Ma = 10$$

T_c

T_h
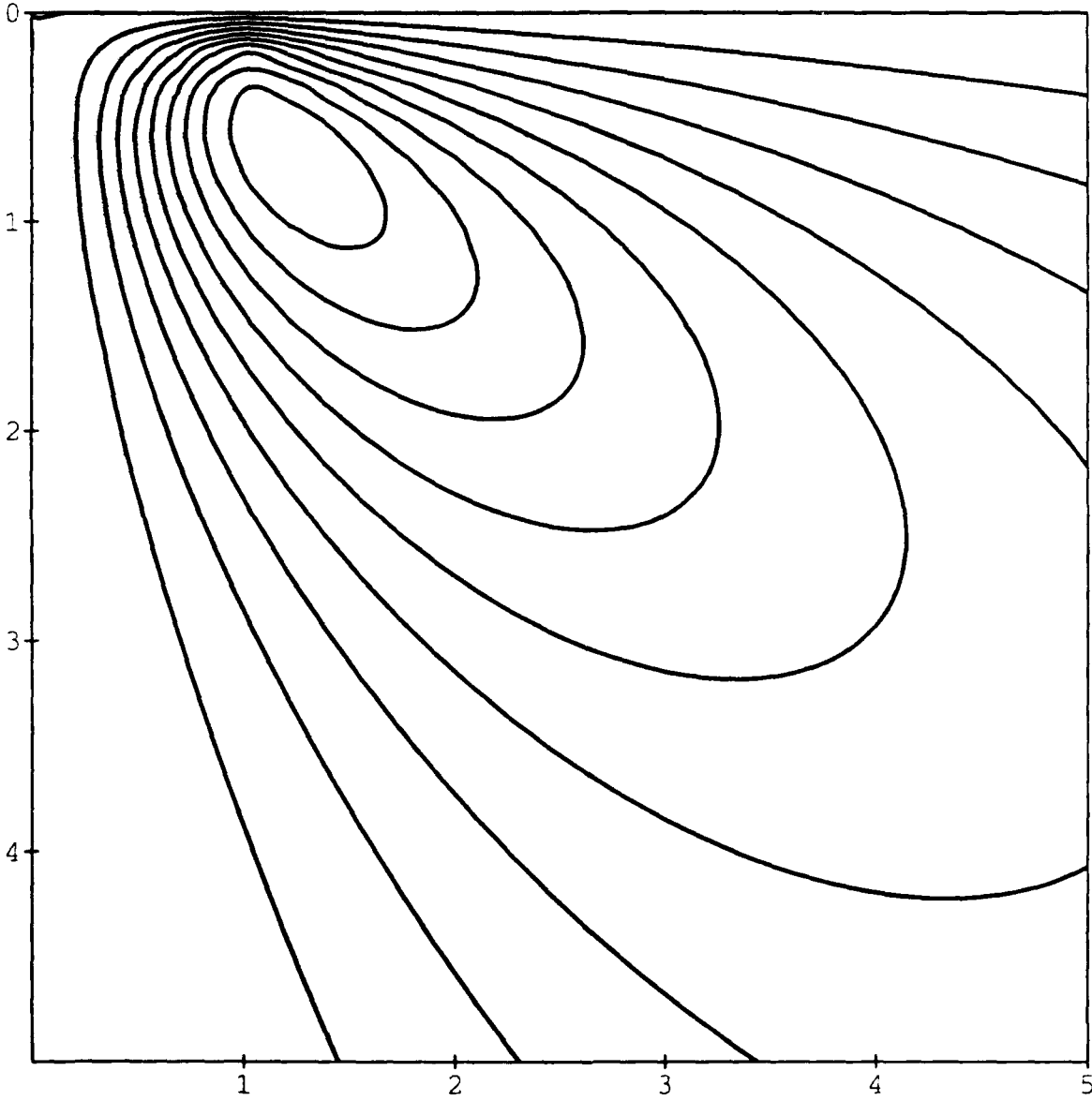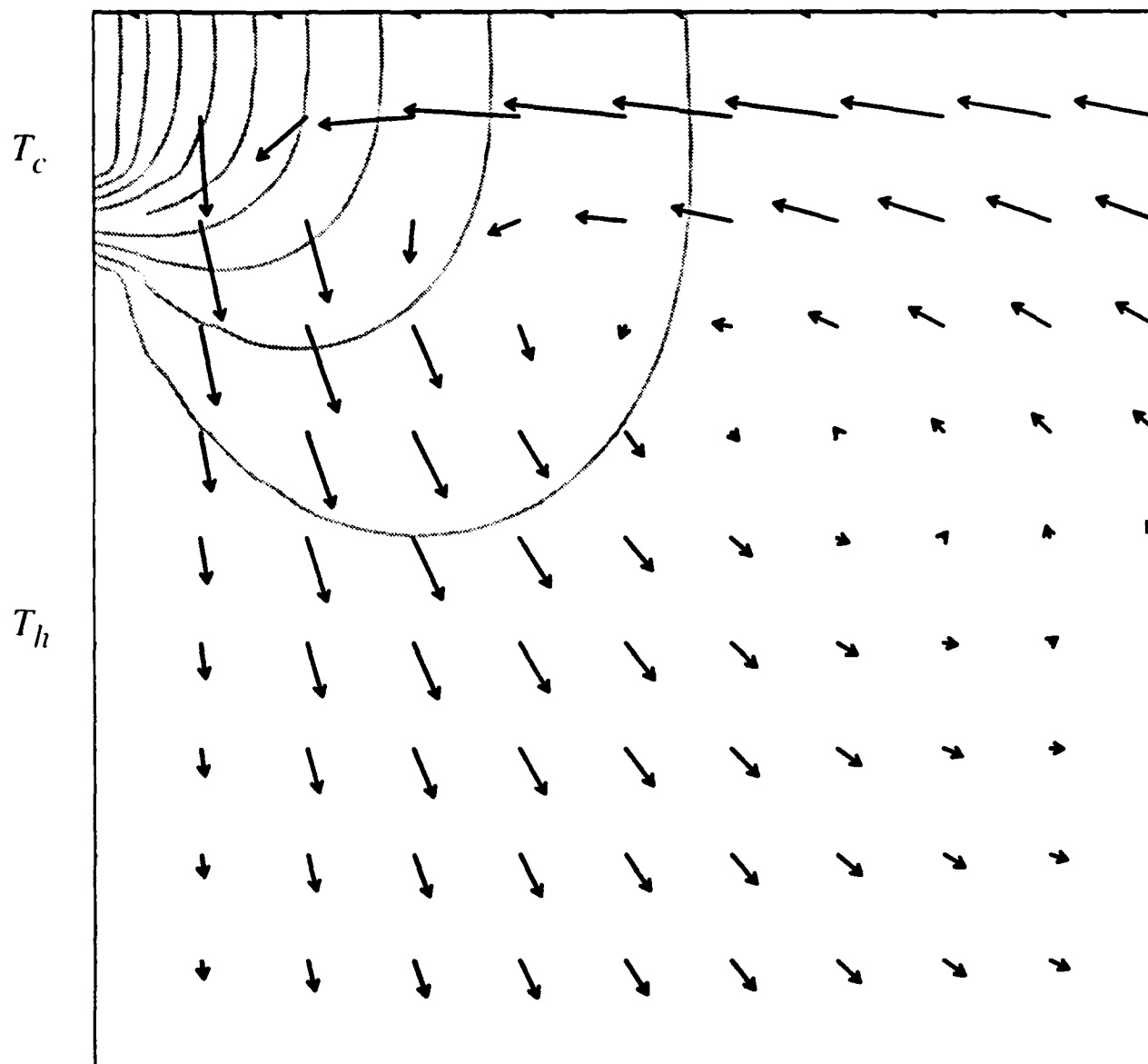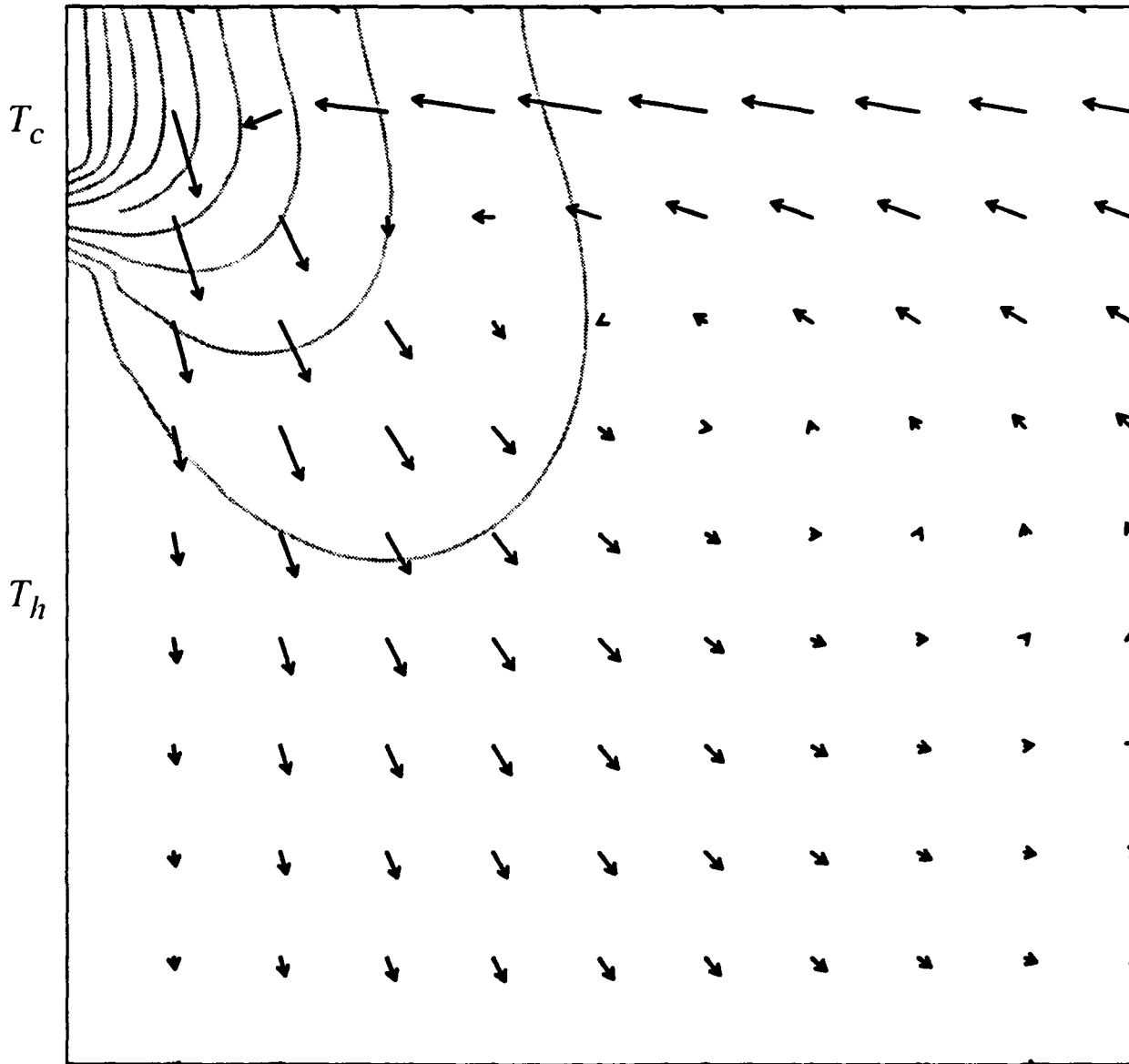
Figure 5b

Ma = 30

Figure 5c

$Ma = 100$
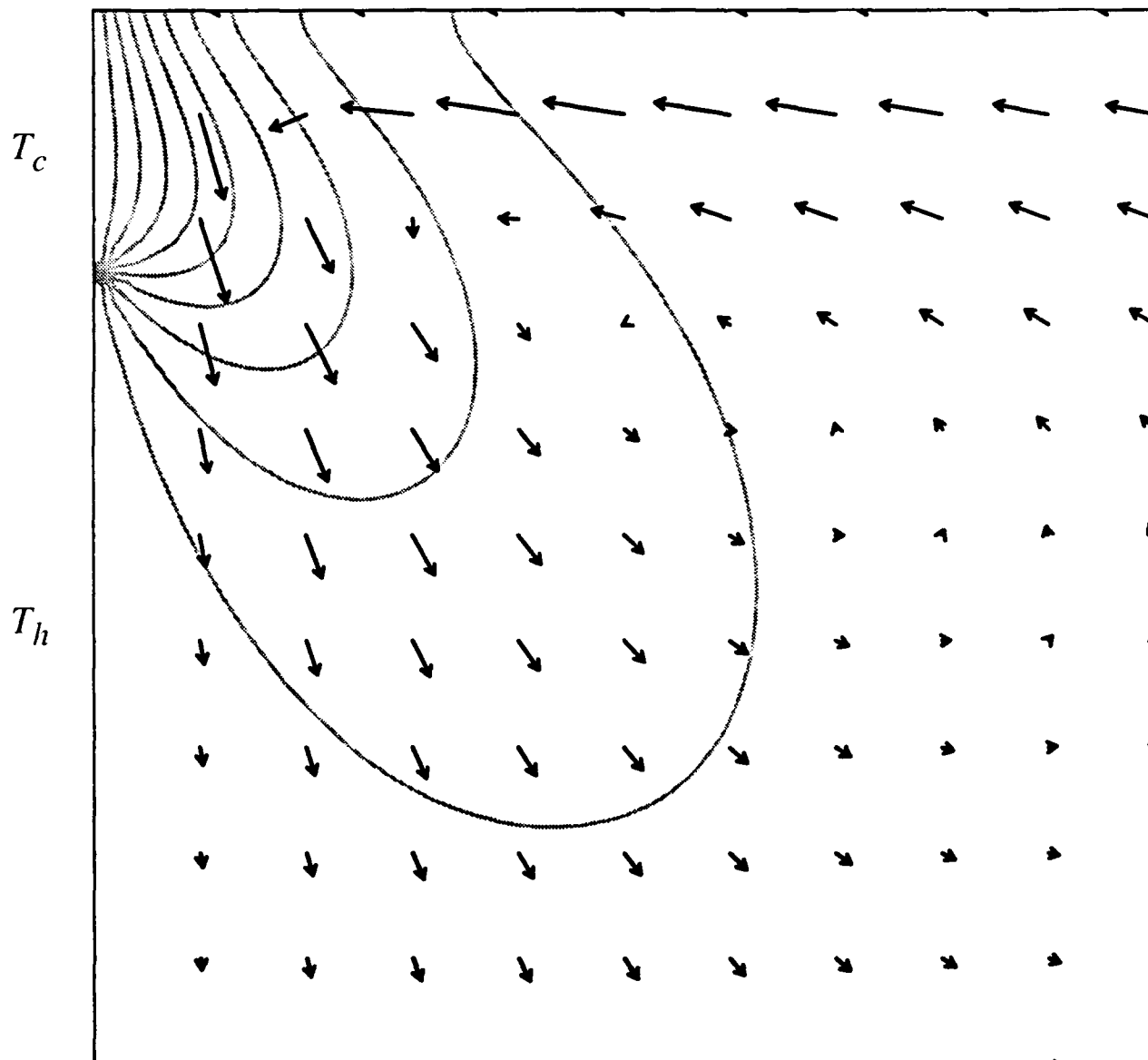
Figure 5d

$$Ma = 300$$

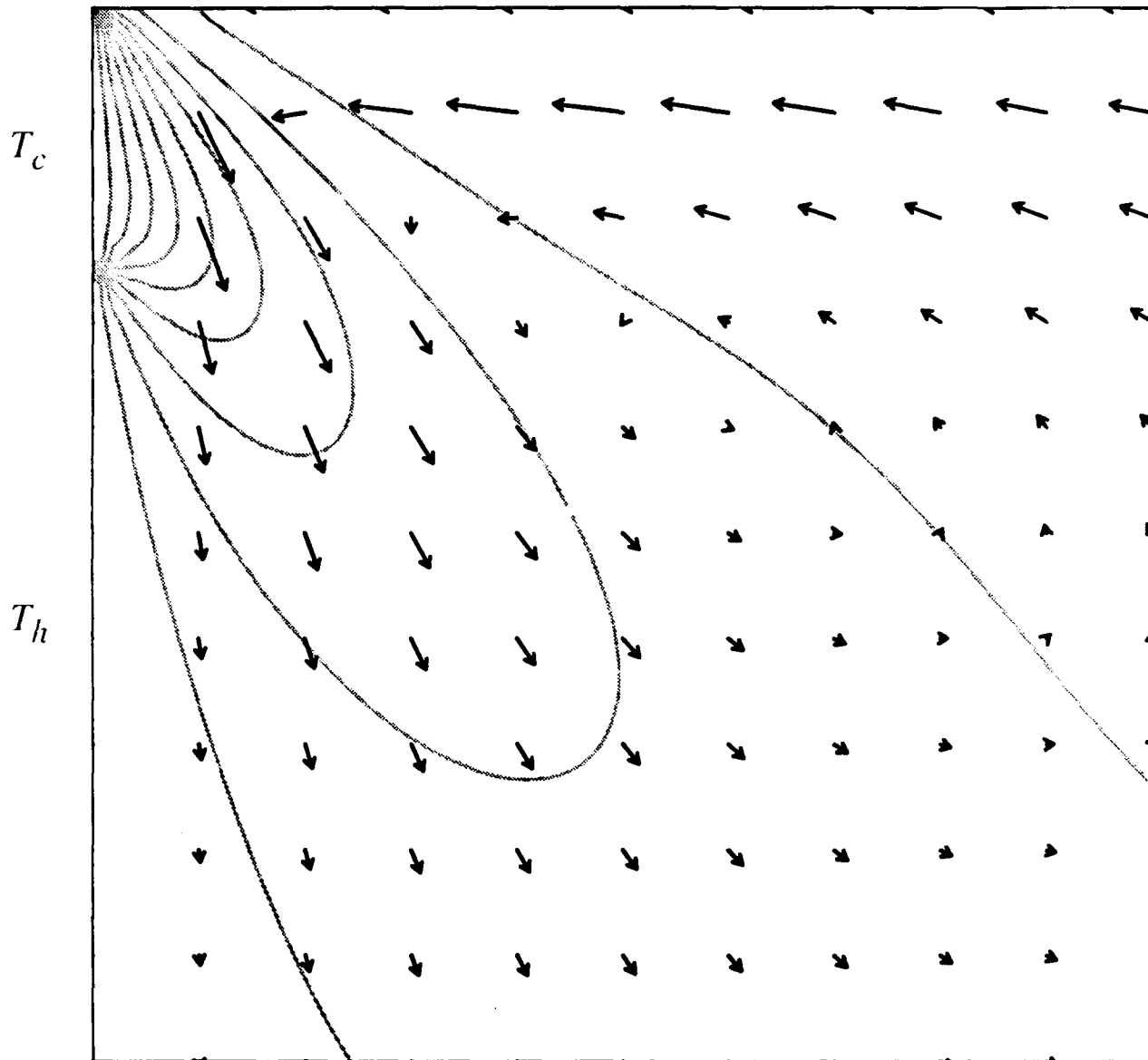Figure 5e
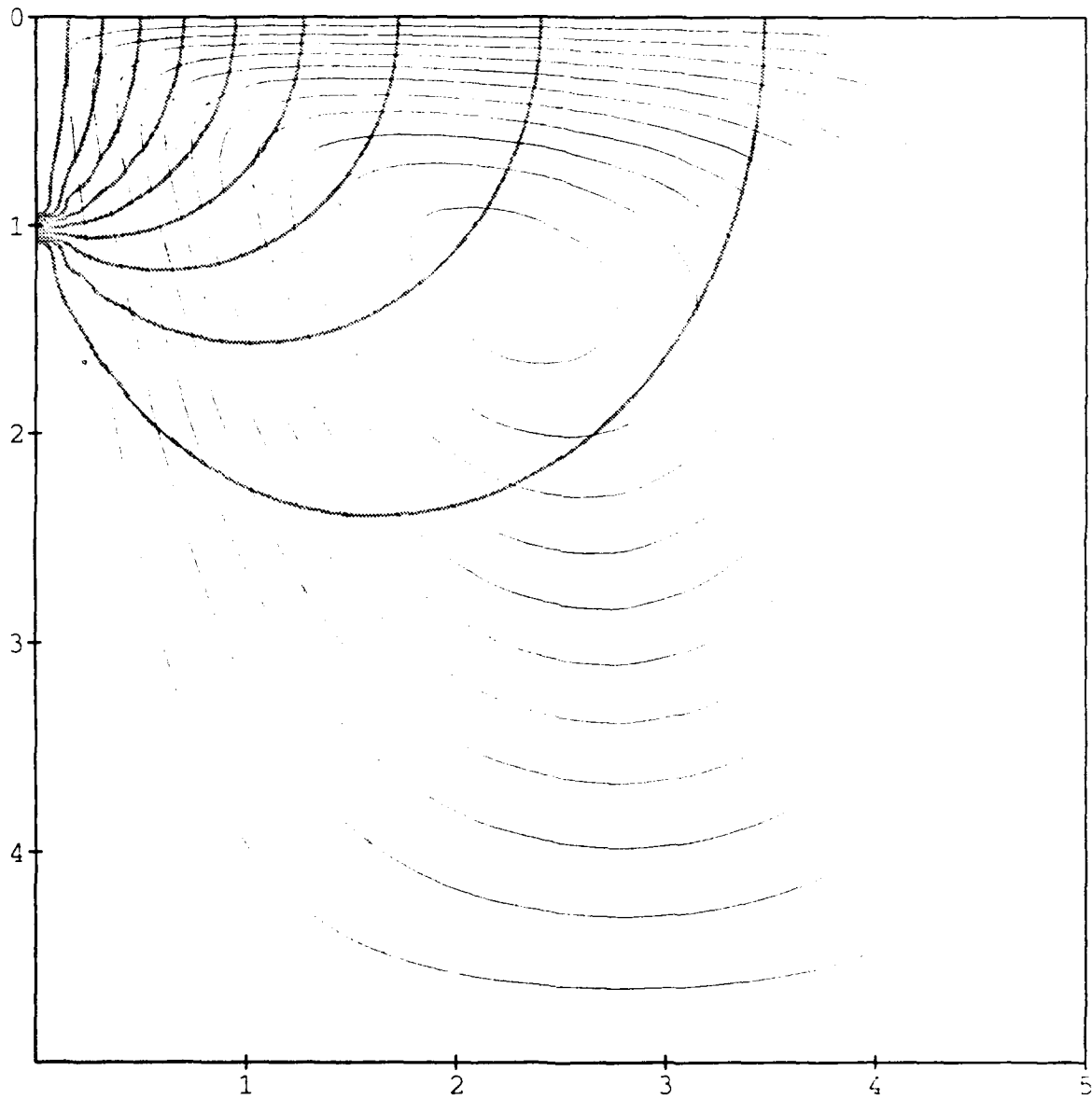
$$Ma = 1000$$

T_c

T_h
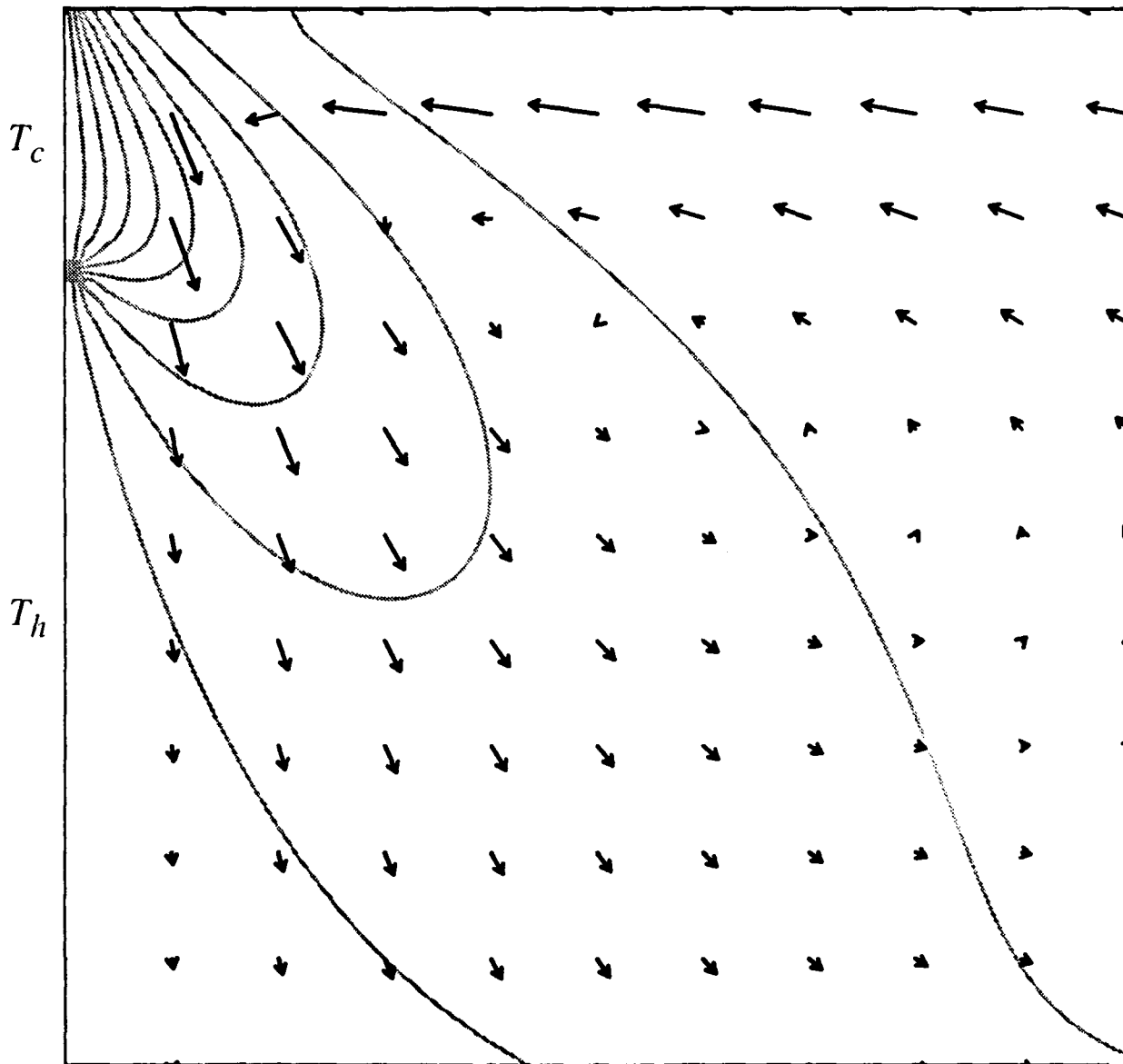
Figure 6a

$M = 0.01, P = 1$
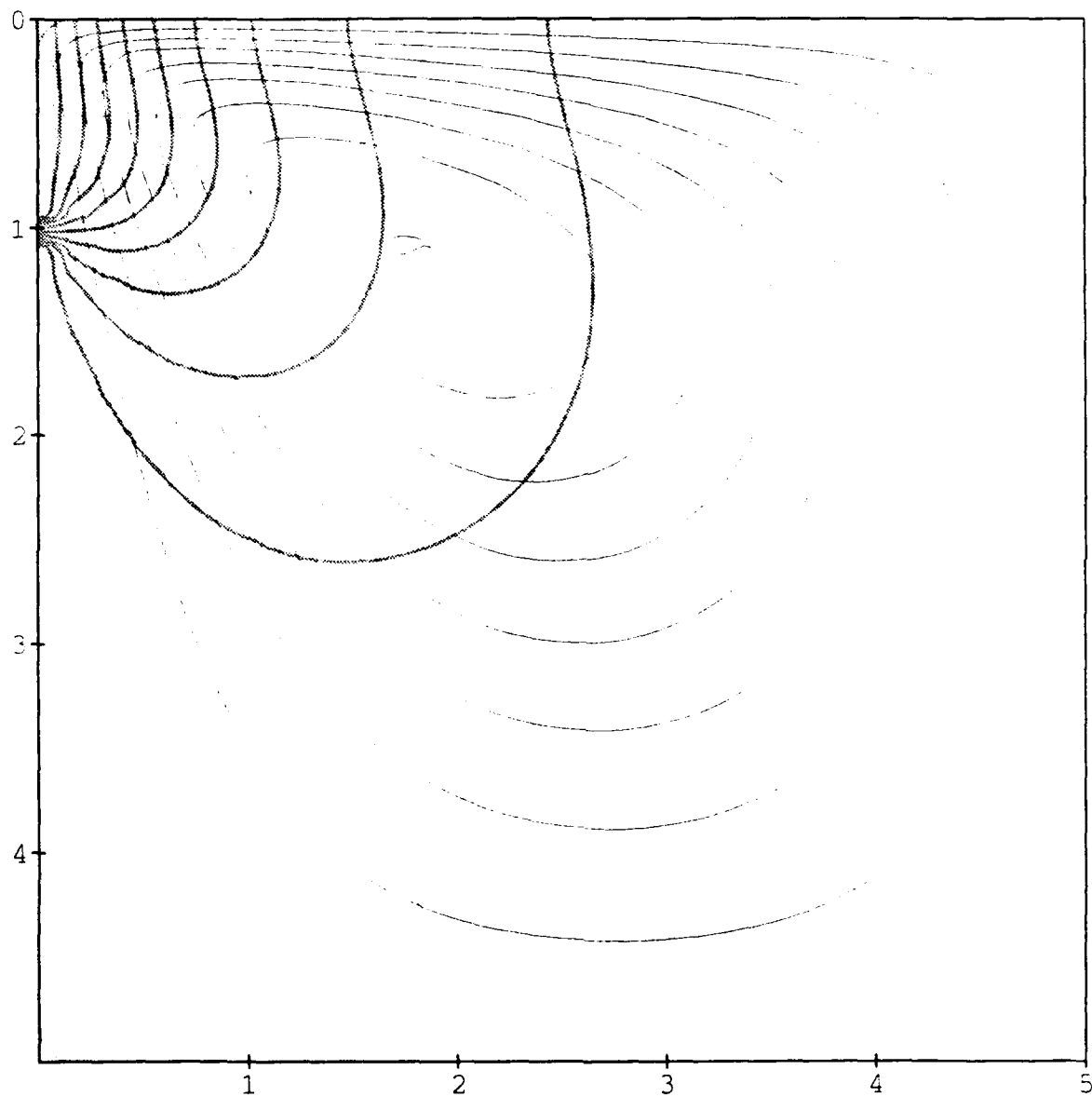
Figure 6b

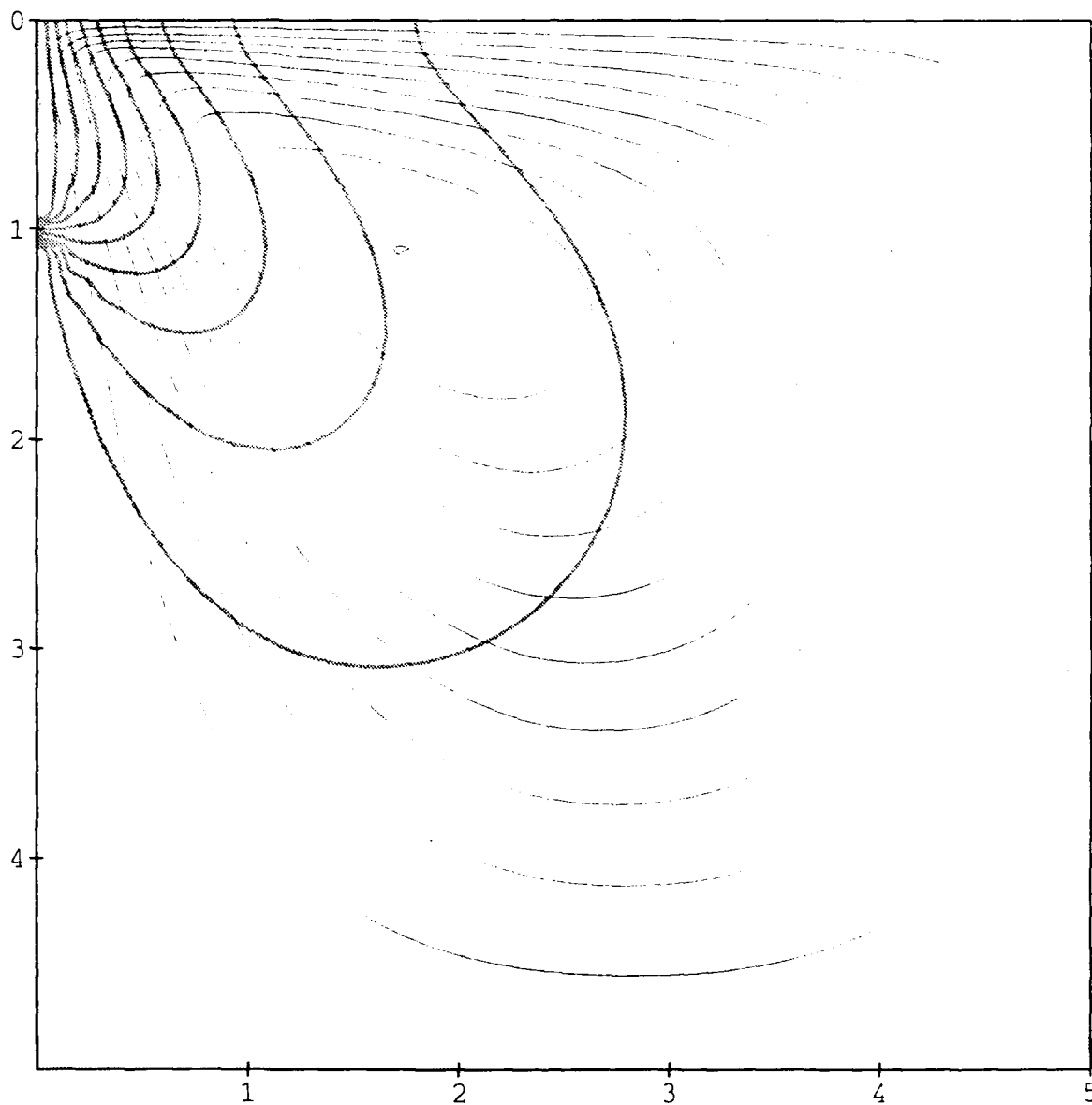## $M = 10, P = 1$
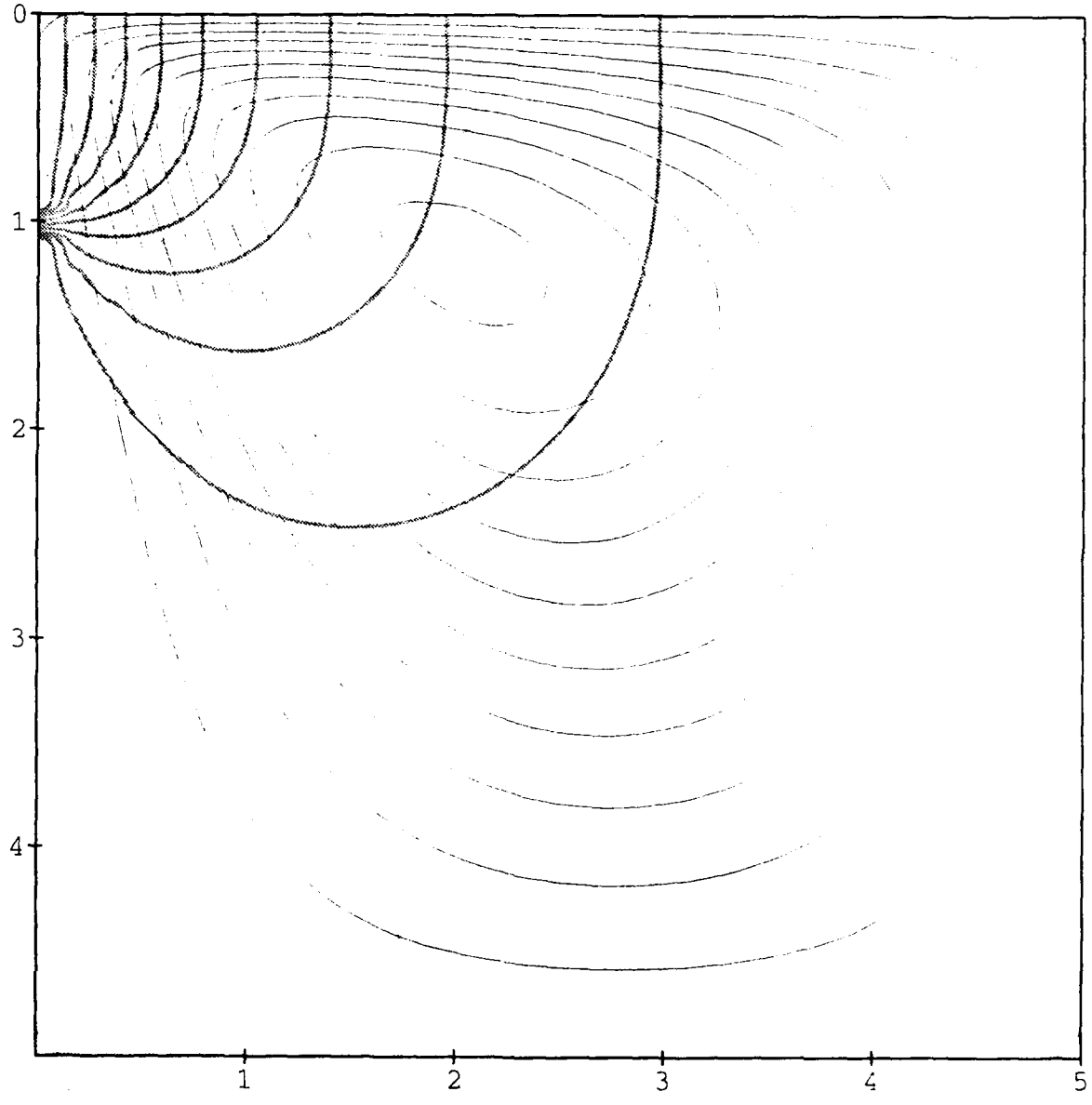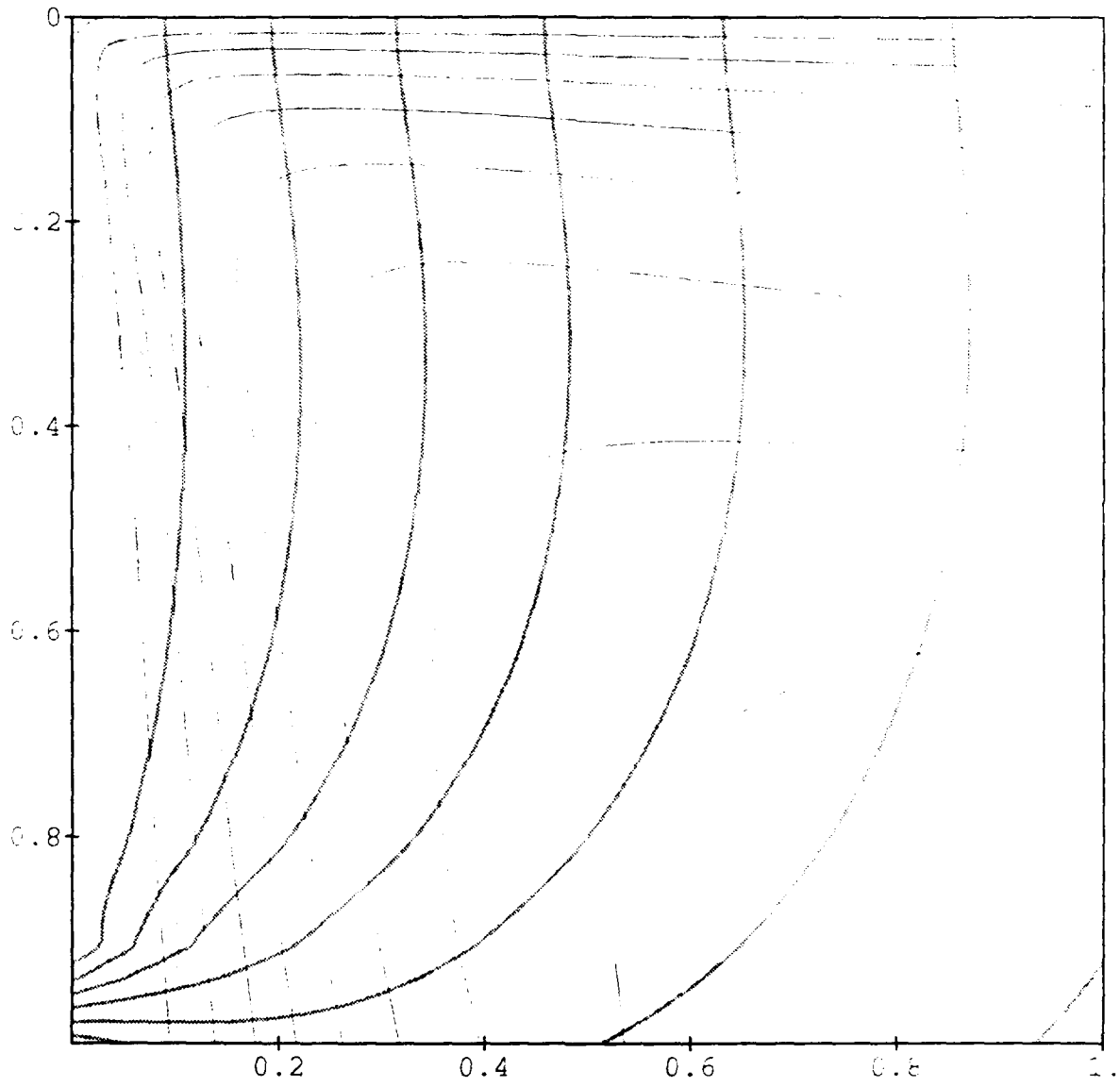
Figure 6c

$$M = 30, P = 1$$

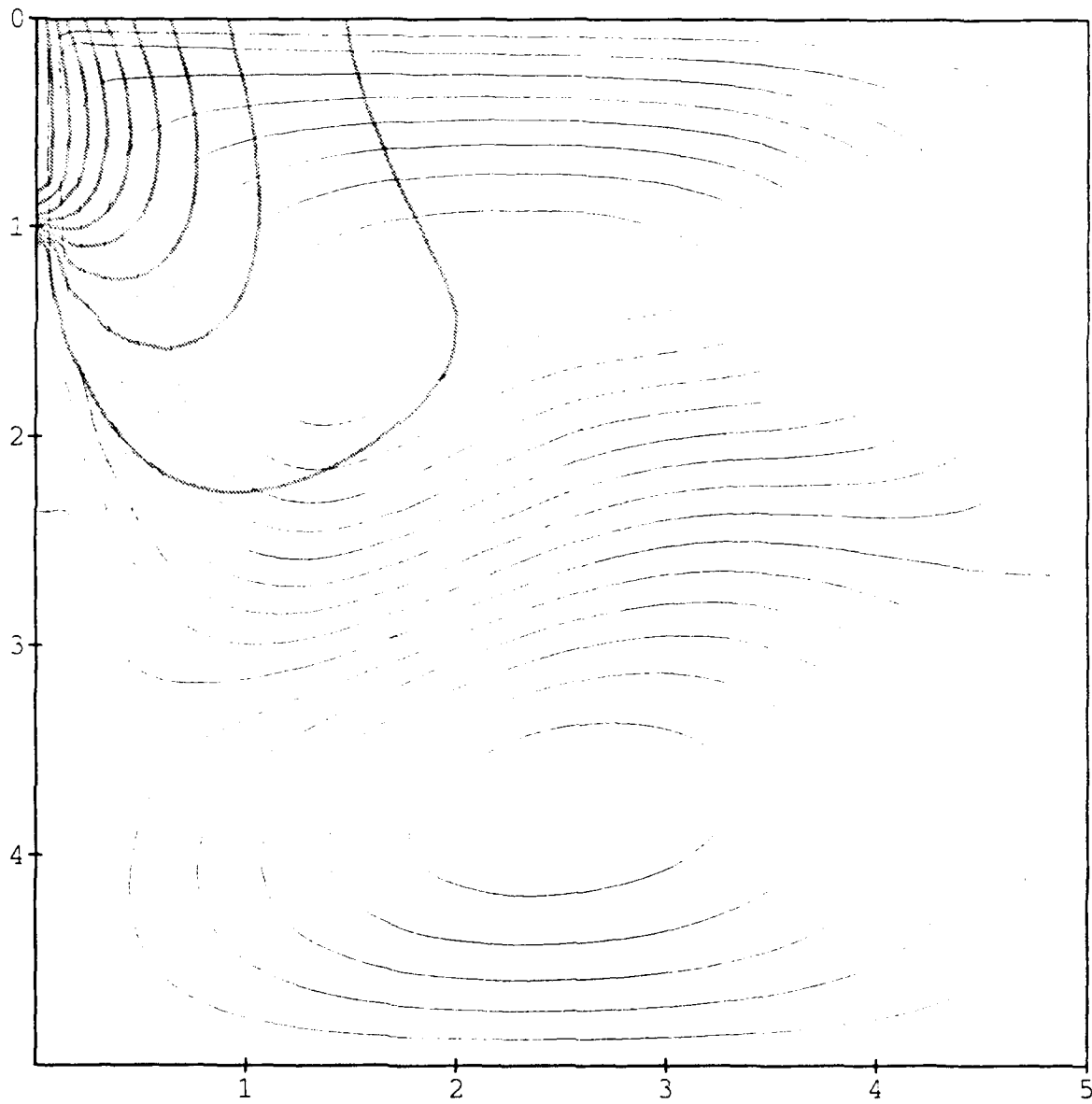Figure 6d

$$M = 100, P = 1$$

Figure 6e

$$M = 300, P = 1$$
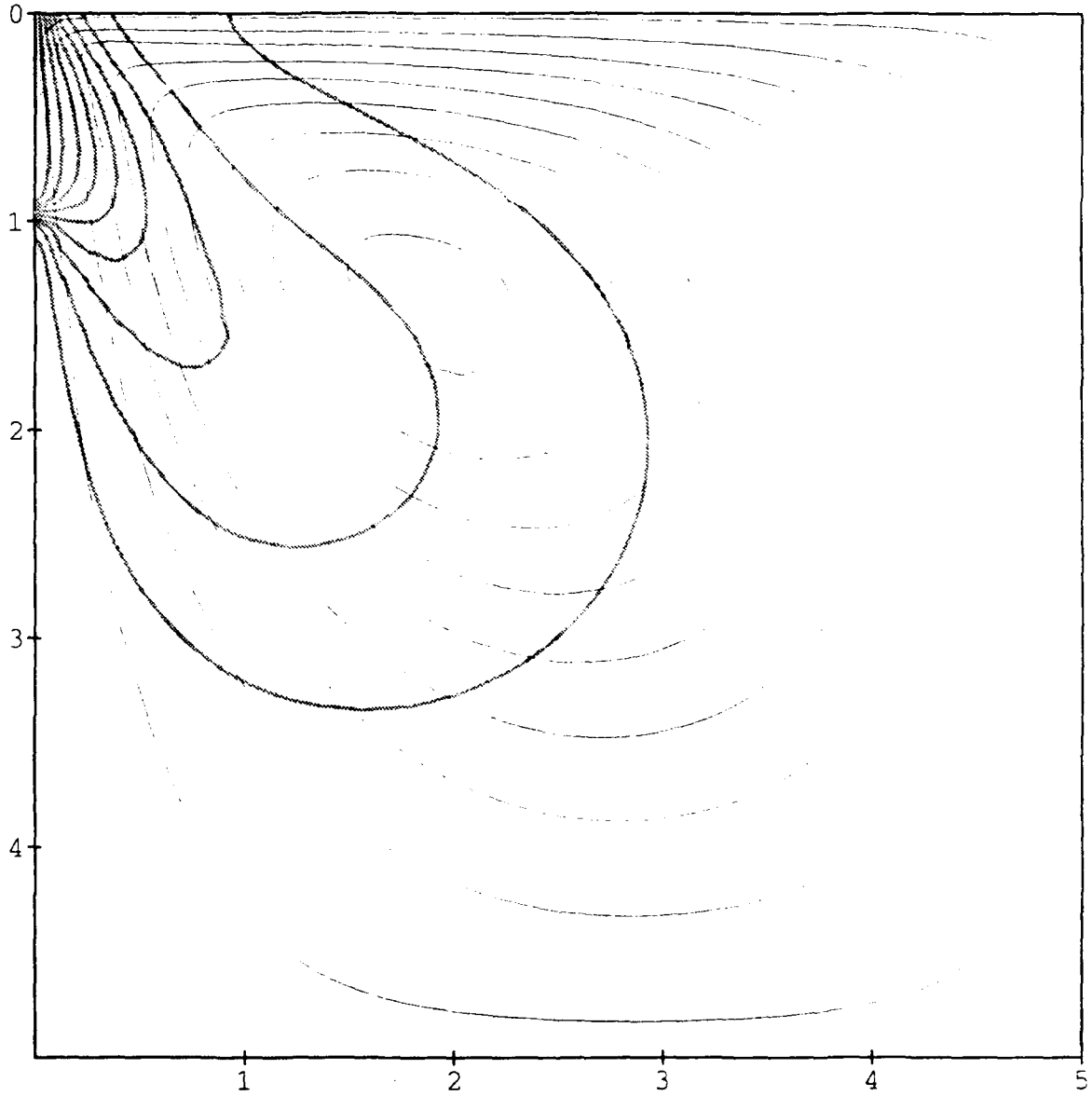
Figure 6f

$$M = 1000, P = 1$$
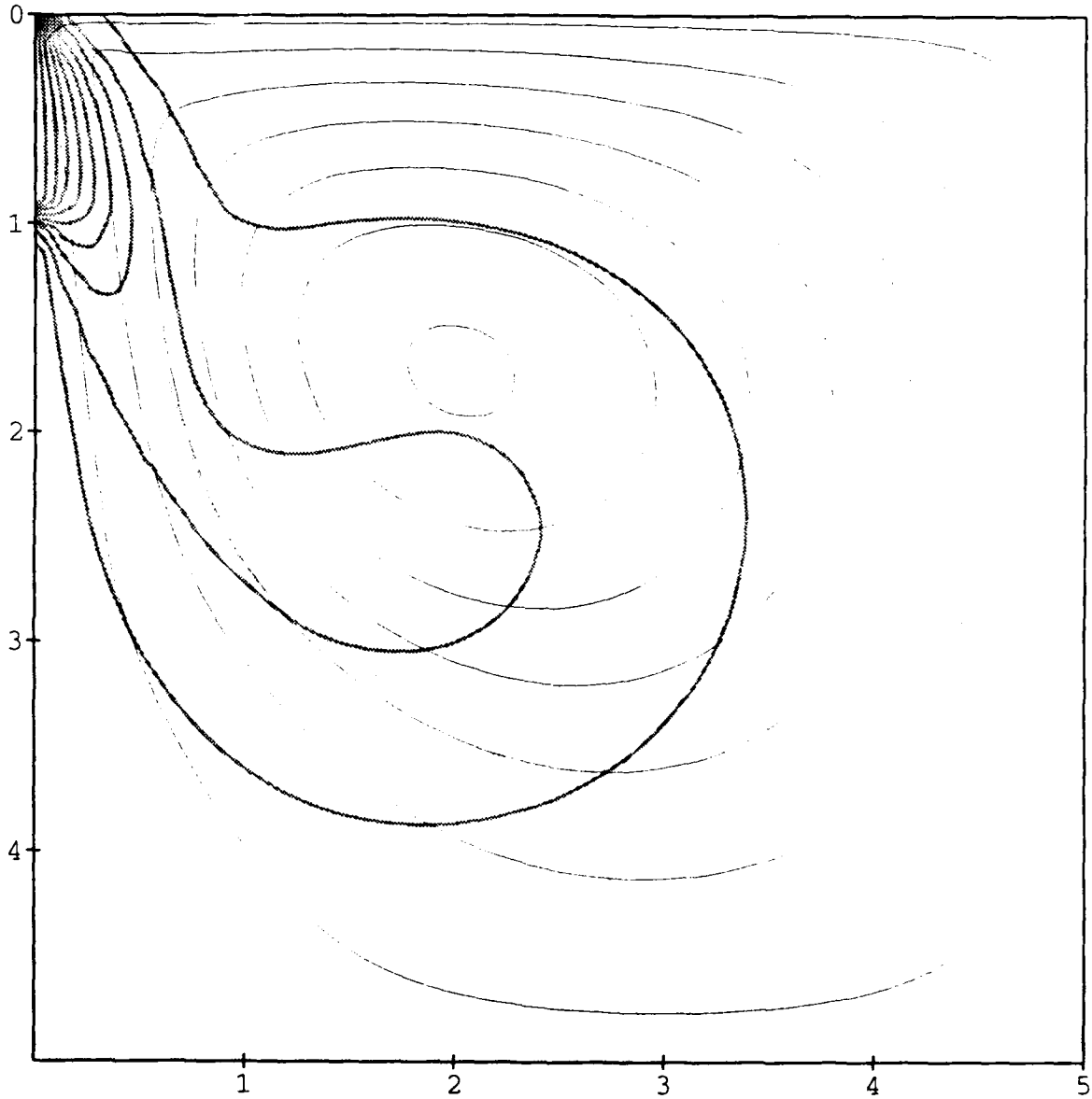
Figure 6g

$$M = 1000, P = 1$$
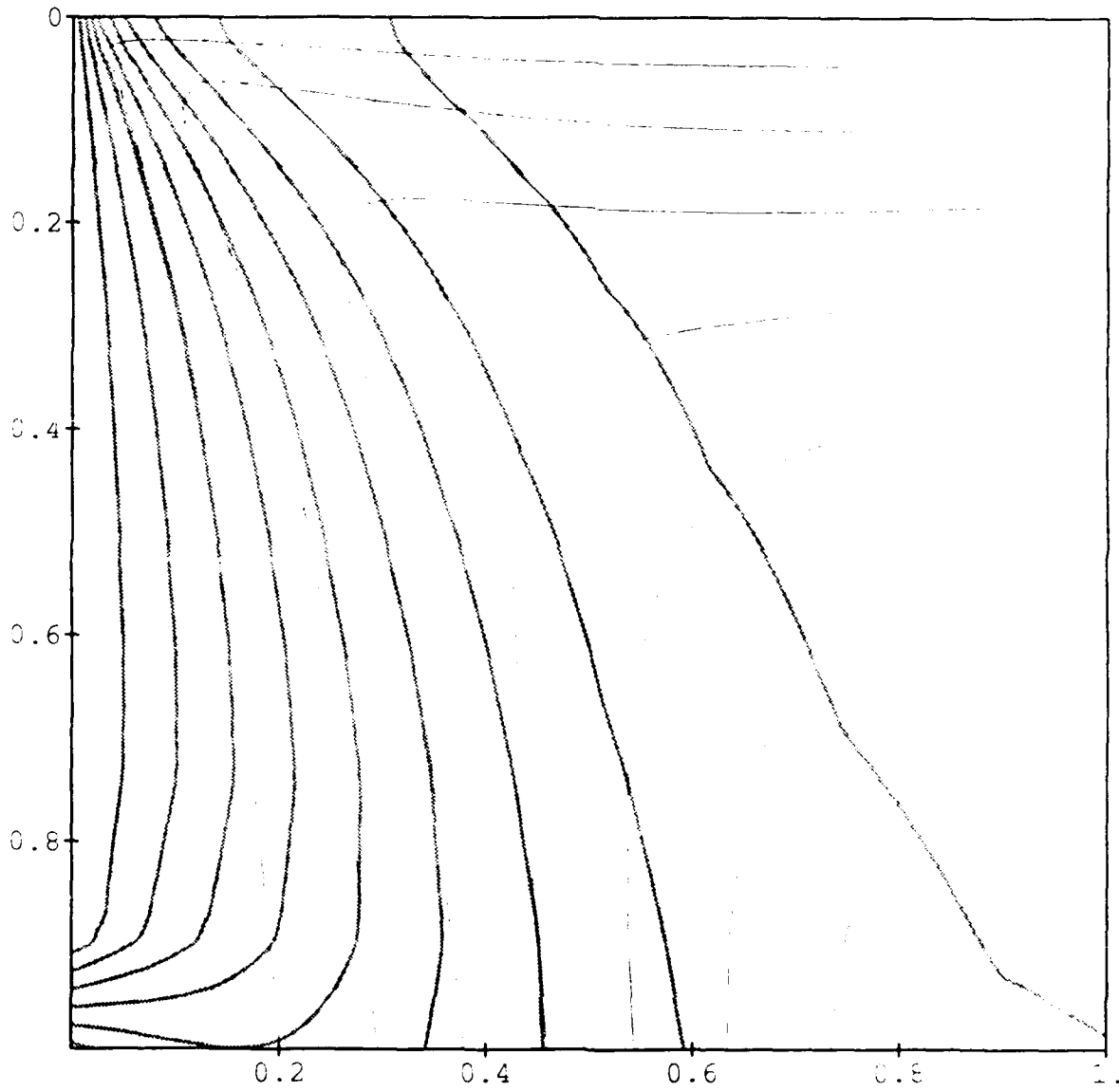
Figure 7a

$$M = 1, P = 0.01$$
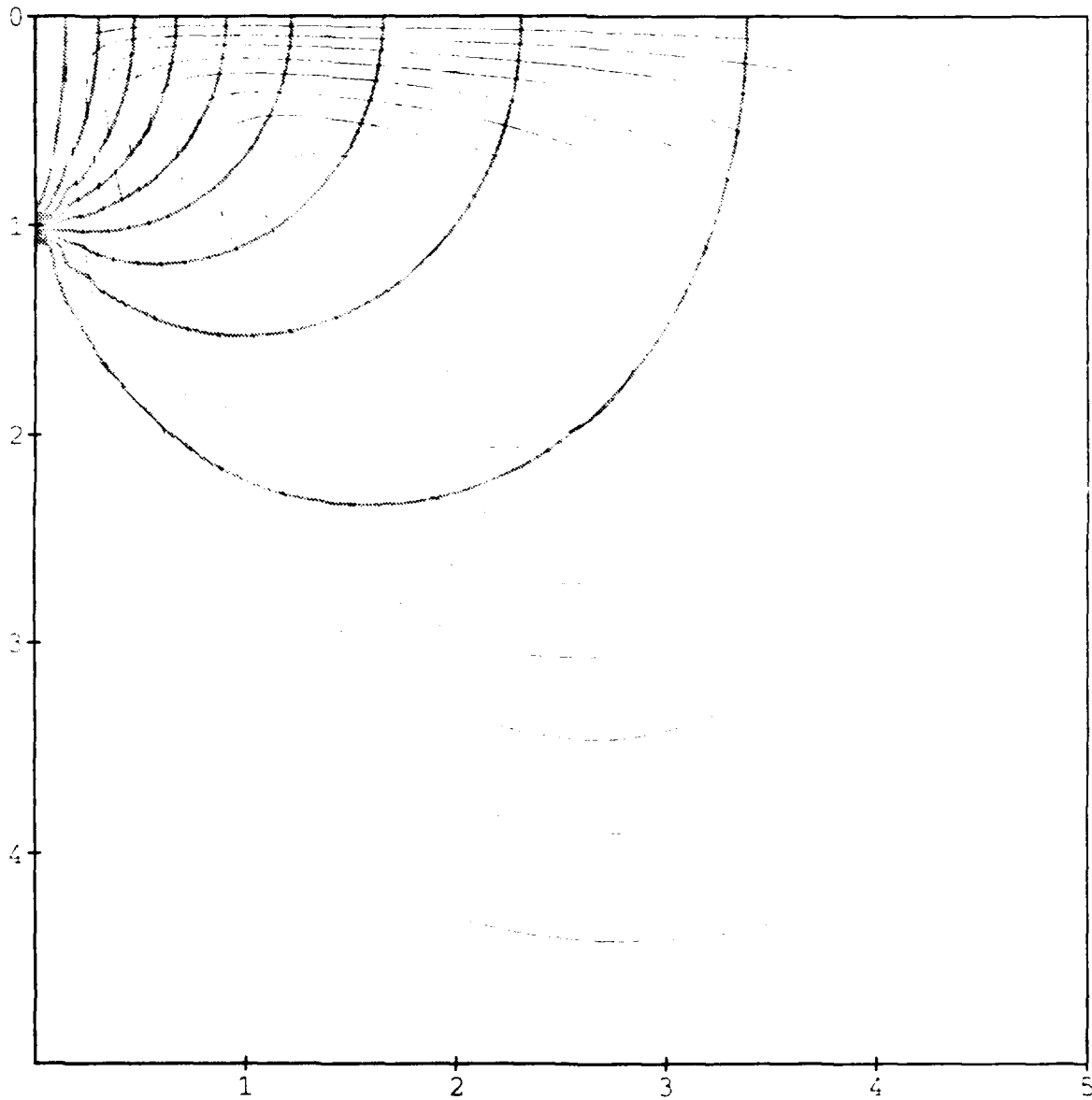
Figure 7b

$M = 10, P = 0.01$
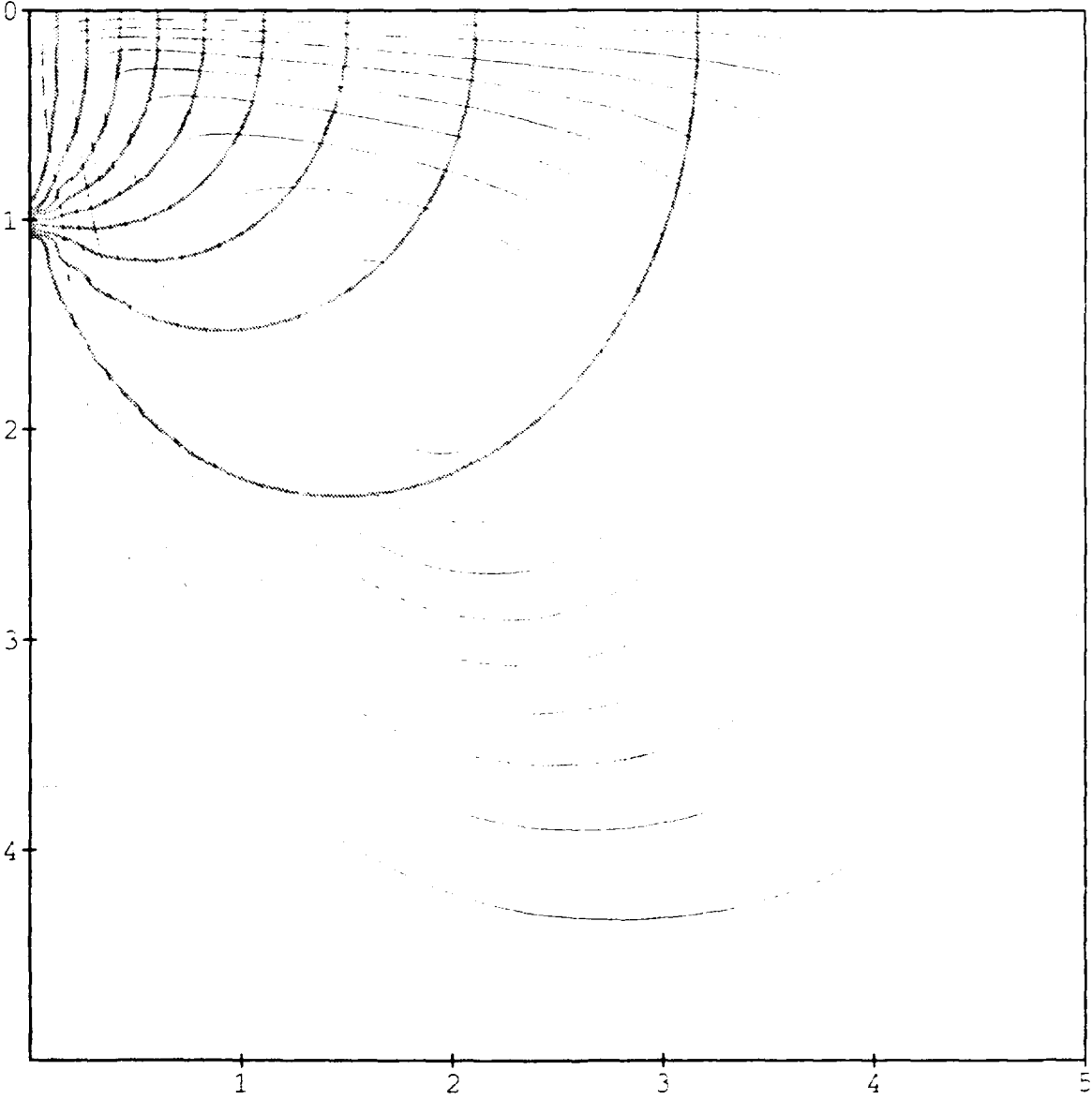
Figure 7c

$$M = 100, P = 0.01$$
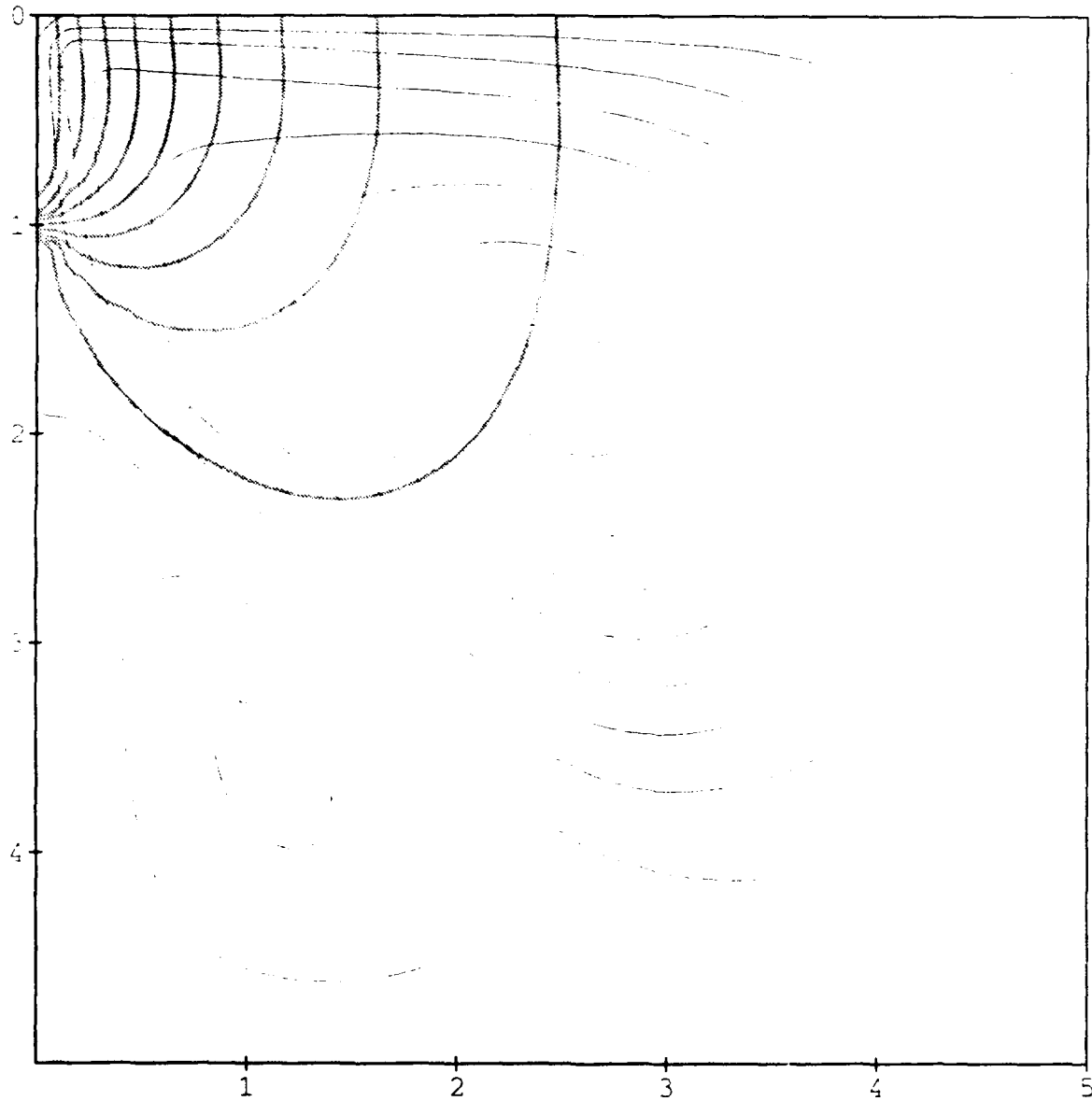
Figure 7d

$M = 100, P = 0.01$

Figure 7e

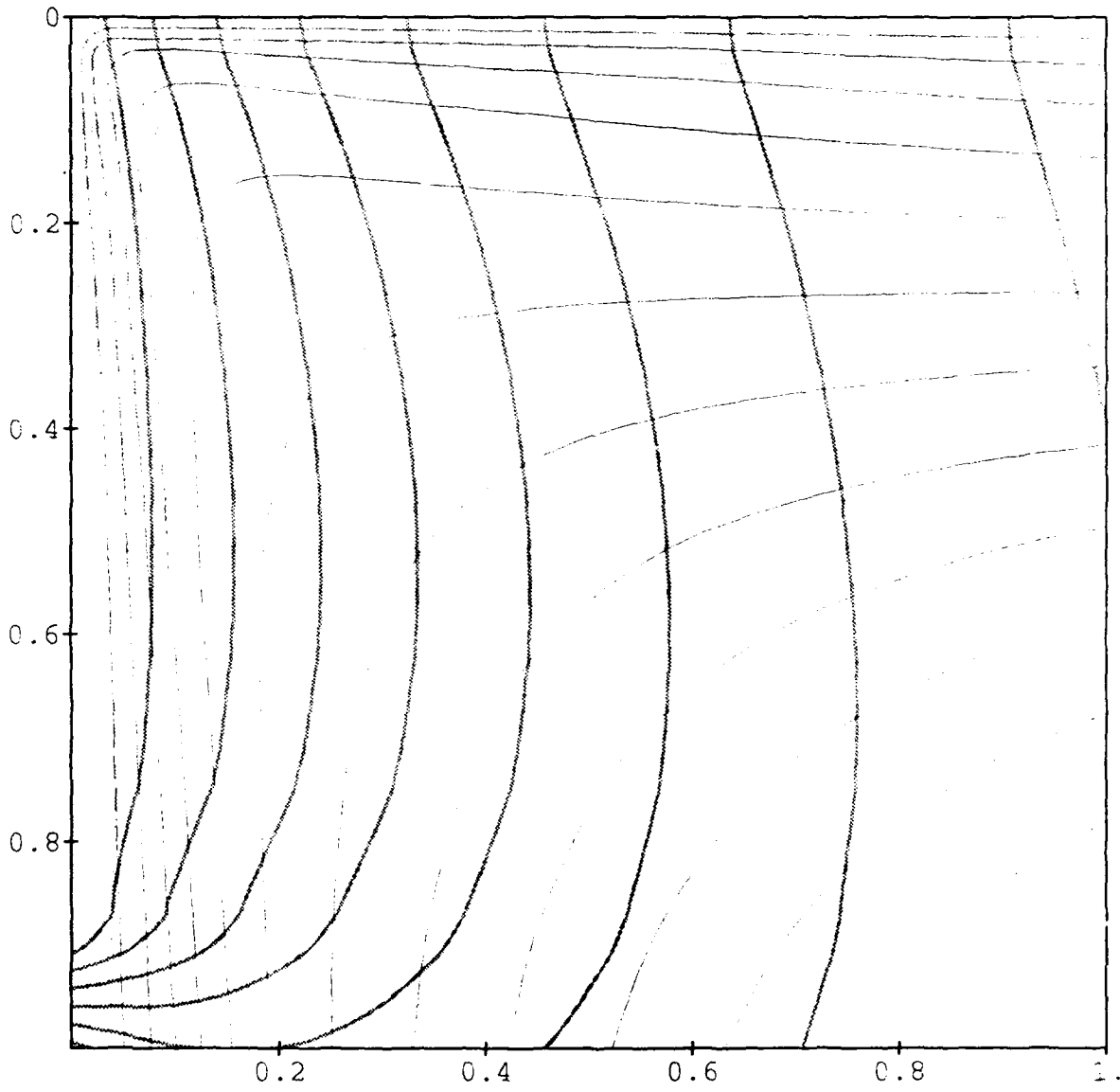$$M = 1000, P = 0.01$$

Figure 7f

$M = 1000, P = 0.01$

Figure 7g

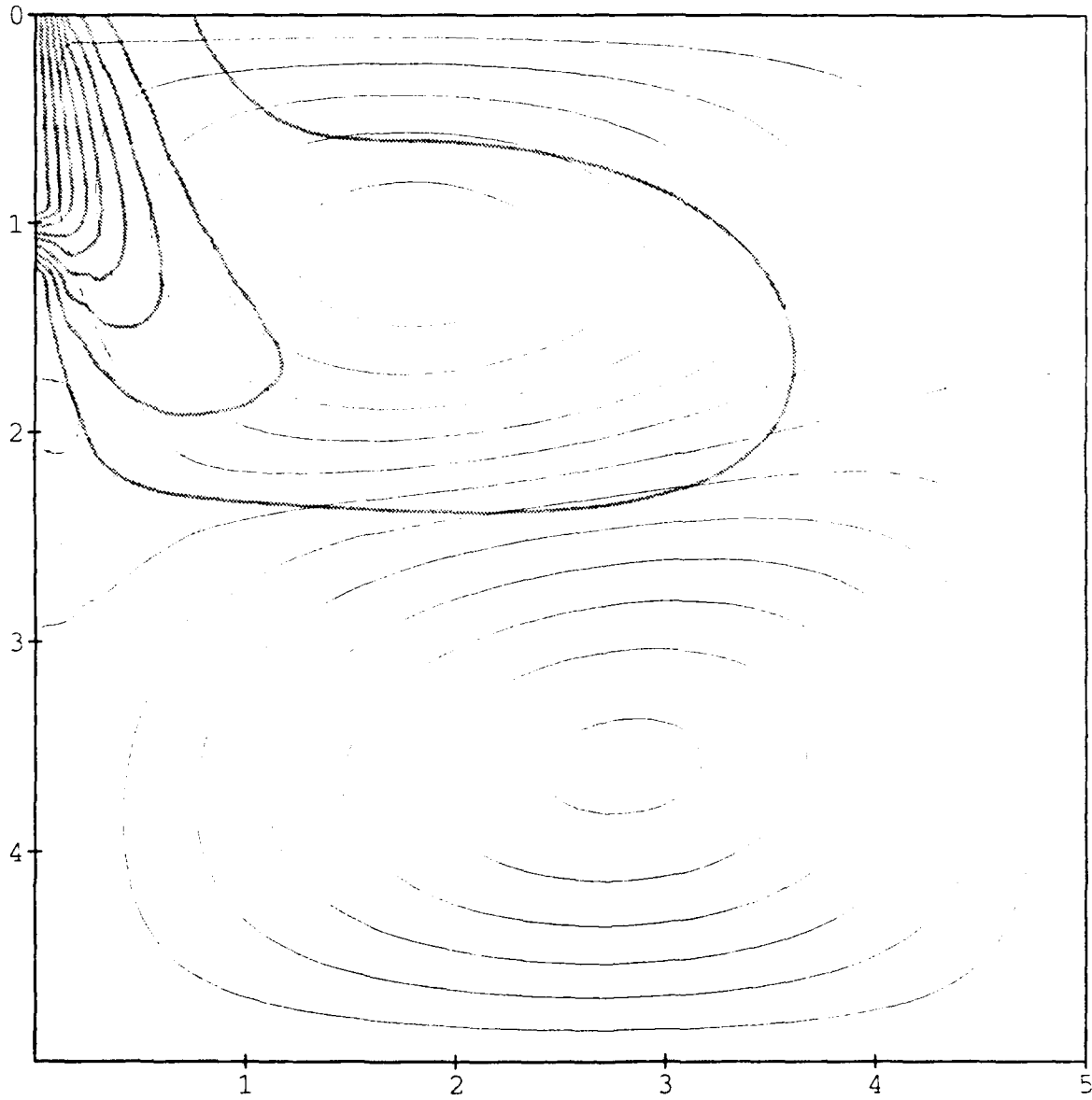## $M = 10000, P = 0.01$

Figure 7h

$M = 10000, P = 0.01$

Figure 8a

Figure 8b

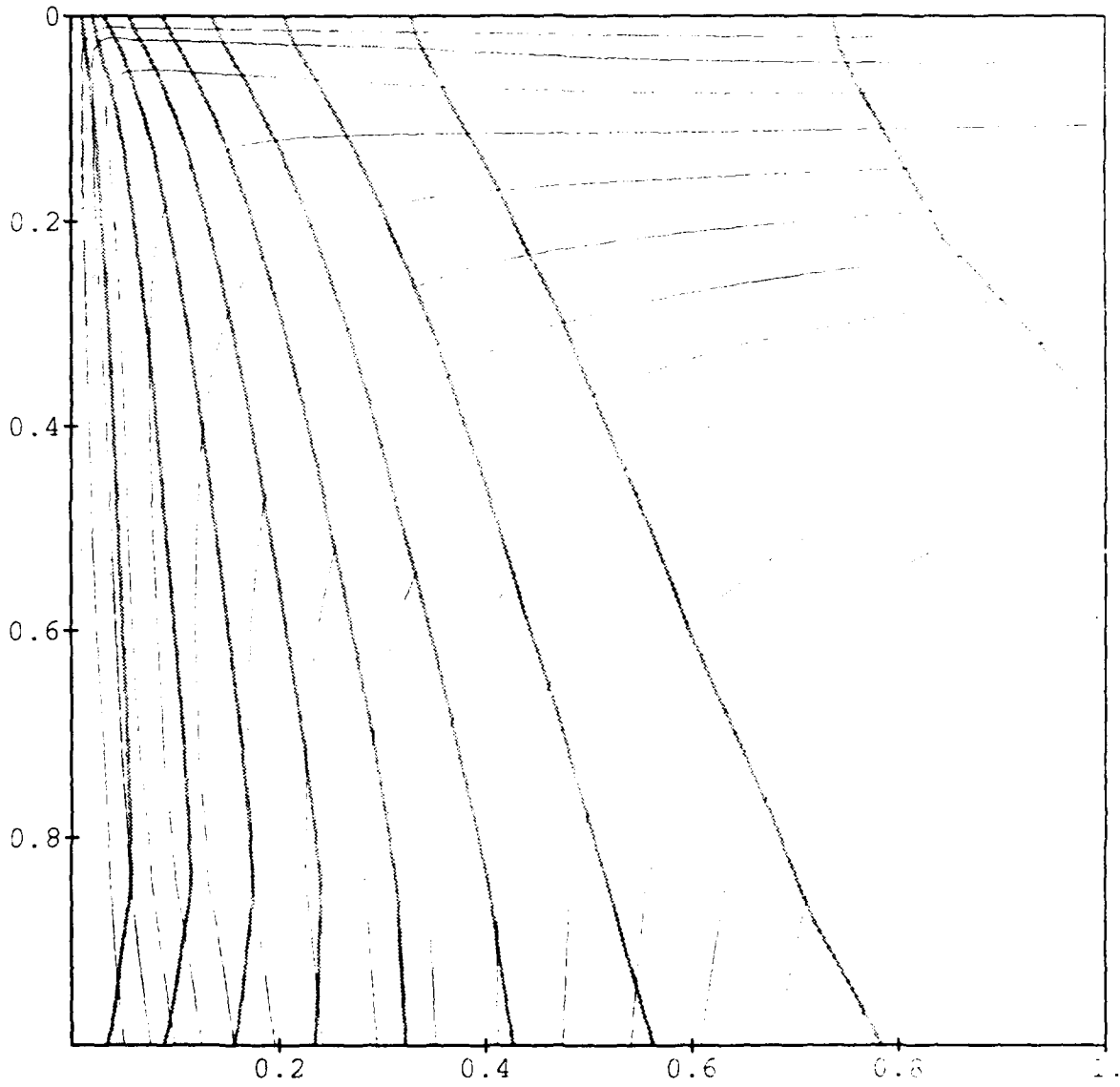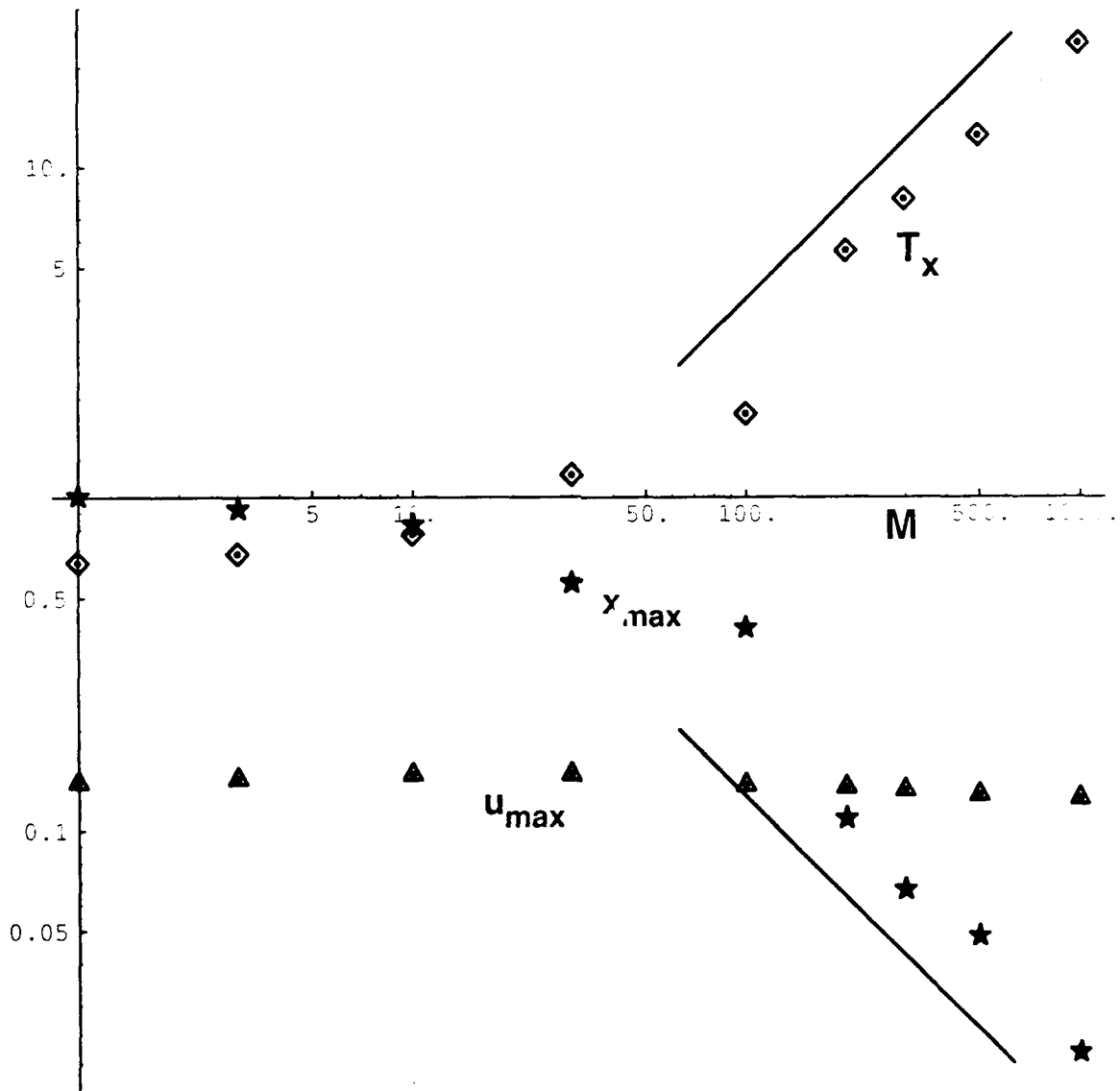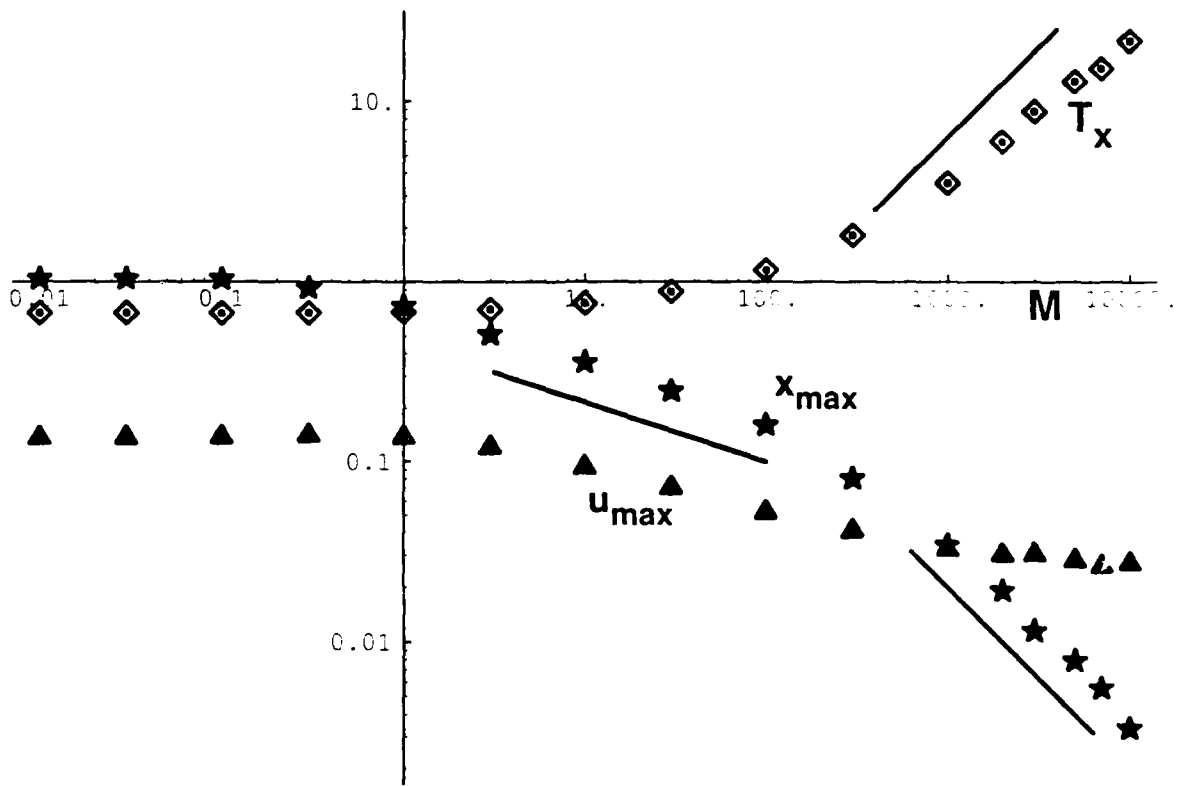## DISTRIBUTION LIST

Director   (2)
Defense Tech Information Center
Cameron Station
Alexandria, VA 22314

Research Office   (1)
Code 81
Naval Postgraduate School
Monterey, CA 93943

Library   (2)
Code 52
Naval Postgraduate School
Monterey, CA 93943

Professor Richard Franke   (1)
Department of Mathematics
Naval Postgraduate School
Monterey, CA 93943

Dr. Neil L. Gerr   (1)
Mathematical Sciences Division
Office of Naval Research
800 North Quincy Street
Arlington, VA 22217-5000

Dr. Richard Lau   (1)
Mathematical Sciences Division
Office of Naval Research
800 North Quincy Street
Arlington, VA 22217-5000

George Yoder   (5)
Office of Naval Research
800 North Quincy St
Arlington, VA 22217-5660

Professor David Canright   (15)
Department of Mathematics
Naval Postgraduate School
Monterey, CA 93943